Title

Orai mediated Calcium entry determines activity of central dopaminergic neurons by regulation of gene expression

Authors

Rishav Mitra[1], Shlesha Richhariya[1,2], Gaiti Hasan[1]

[1] National Centre for Biological Sciences, Tata Institute of Fundamental Research, Bangalore, India
[2] Department of Biology, Brandeis University, Waltham, USA

Correspondence: gaiti@ncbs.res.in

Keywords

Neuromodulation, Drosophila flight, PPL1 DANs, histone modifications, Trithorax-like, GAF

Highlights

1. Store-operated Ca^{2+} entry (SOCE) through Orai is required in a set of flight-promoting central dopaminergic neurons (fpDANs) during late pupae and early adults to establish their gene expression profile.

2. SOCE activates a homeobox transcription factor, '*Trithorax-like*' and thus regulates expression of histone modifiers Set2 and *E(z)* to generate a balance between opposing epigenetic signatures of H3K36me3 and H3K27me3 on downstream genes.

3. SOCE drives a transcriptional feedback loop to ensure expression of key genes required for neuronal function including the muscarinic acetylcholine receptor (*mAChR*) and the inositol 1,4,5-trisphosphate receptor (*itpr).*

4. The transcriptional program downstream of SOCE is key to functional maturation of the dopaminergic neurons, enabling their neuronal excitability, axonal arborization and synaptic transmission required for adult flight.

Graphical Abstract

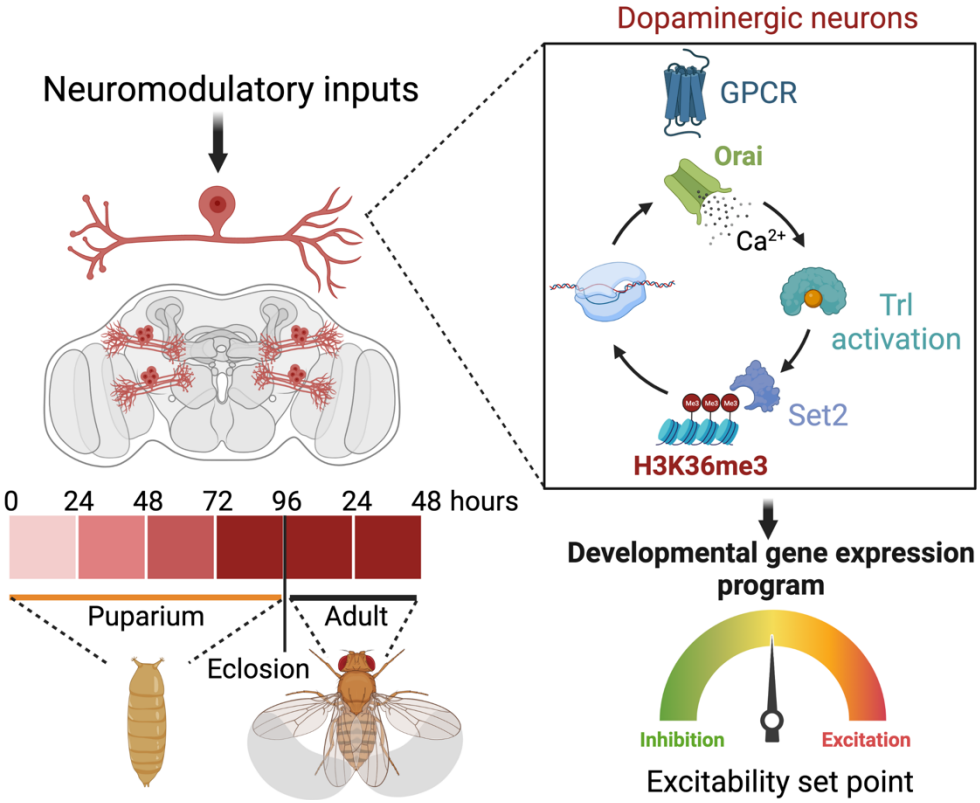

Abstract

Maturation and fine-tuning of neural circuits frequently requires neuromodulatory signals that set the excitability threshold, neuronal connectivity and synaptic strength. Here we present a mechanistic study of how neuromodulator stimulated intracellular Ca^{2+} signals, through the store - operated Ca^{2+} channel Orai, regulate intrinsic neuronal properties by control of developmental gene expression in flight promoting central dopaminergic neurons (fpDANs). The fpDANs receive cholinergic inputs for release of dopamine at a central brain tripartite synapse that sustains flight (Sharma and Hasan, 2020). Cholinergic inputs act on the muscarinic acetylcholine receptor to stimulate intracellular Ca^{2+} release through the endoplasmic reticulum (ER) localised inositol 1,4,5-trisphosphate receptor followed by ER-store depletion and Orai mediated store-operated Ca^{2+} entry (SOCE). Analysis of gene expression in fpDANs followed by genetic, cellular and molecular studies identified Orai-mediated Ca^{2+} entry as a key regulator of excitability in fpDANs during circuit maturation. SOCE activates the transcription factor Trithorax-like (Trl) which in turn drives expression of a set of genes including *Set2*, that encodes a histone 3 Lysine 36 methyltransferase (H3K36me3). Set2 function establishes a positive feedback loop,

essential for receiving neuromodulatory cholinergic inputs and sustaining SOCE. Chromatin modifying activity of Set2 changes the epigenetic status of fpDANs and drives expression of key ion channel and signaling genes that determine fpDAN activity. Loss of activity reduces the axonal arborisation of fpDANS within the MB lobe, and prevents dopamine release required for maintenance of long flight.

Introduction

Neural circuitry underlying mature adult behaviours emerges from a combination of developmental gene expression programs and experience-dependent neuronal activity. Holometabolous insects such as *Drosophila*, reconfigure their nervous system during metamorphosis to generate circuitry capable of supporting adult behaviours (Levine, 1984). During pupal development, neurons undergo maturation of their electrical properties with a gradual increase in depolarizing responses and consequent synaptic transmission (Hardie et al., 1993; Jarvilehto and Finell, 1983). Apart from voltage-gated Ca^{2+} channels and fast-acting neurotransmitters specific to ionotropic receptors, the developing nervous system also uses neuromodulators, that target metabotropic receptors, show slower response kinetics and are capable of affecting a larger subset of neurons by means of diffusion aided volumetric transmission (Taber and Hurley, 2014). Although neuromodulators alter intrinsic neuronal properties (Marder, 2012) by changes in gene expression, the molecular mechanisms through which this is achieved and maintained over developmental timescales needs further understanding.

Ca^{2+} signals generated by neuronal activity can determine neurotransmitter specification (Spitzer, 2012), synaptic plasticity (O'Hare et al., 2022; Takechi et al., 1998), patterns of neurite growth (Gu and Spitzer, 1995) and gene expression programs (Ciceri et al., 2022; Rosenberg and Spitzer, 2011) over developmental timescales (McKinney et al., 2022) where output specificity is defined by signal dynamics. Neuromodulators generate intracellular Ca^{2+} signals by stimulation of cognate G-Protein Coupled Receptors (GPCRs) linked to the inositol 1,4,5-trisphosphate (IP_3) and Ca^{2+} signalling pathway. IP_3 transduces intracellular Ca^{2+} release through the endoplasmic reticulum (ER) localised ligand-gated ion channel, the inositol 1,4,5-trisphosphate receptor (IP_3R; Streb et al., 1984), followed by store-operated Ca^{2+} entry (SOCE) through the plasma membrane localised Orai channel

(Prakriya and Lewis, 2015; Thillaiappan et al., 2019). Cellular and physiological consequences of Ca^{2+} signals generated through SOCE exhibit different time-scales and sub-cellular localisation from activity induced signals, suggesting that they alter neuronal properties through novel mechanisms.

Expression studies, genetics and physiological analysis support a role for IP_3/Ca^{2+} and SOCE in neuronal development and the regulation of adult neuronal physiology across organisms (Hasan and Sharma, 2020; Mitra and Hasan, 2022; Somasundaram et al., 2014). In *Drosophila*, neuromodulatory signals of neurotransmitters and neuropeptides stimulate cognate GPCRs on specific neurons to generate IP_3 followed by intracellular Ca^{2+} release and SOCE (Agrawal et al., 2013; Megha and Hasan, 2017; Shakiryanova et al., 2011). Genetic and cellular studies identified neuromodulatory inputs and SOCE as an essential component for maturation of neural circuits for flight (Pathak et al., 2015; Venkiteswaran and Hasan, 2009). A focus of this flight deficit lies in a group of central dopaminergic neurons (or DANs) that include the PPL1 and PPM3 DANs (Liu et al. 2012) marked by *THD' GAL4,* alternately referred to henceforth as flight promoting DANs (fpDANs). Among the fpDANs some PPL1 DANs project to the γ2α'1 lobe of the Mushroom Body (MB; Mao and Davis 2009) a dense region of neuropil in the insect central brain, that forms a relay centre for flight (Sharma and Hasan, 2020). Axonal projections from Kenyon cells (KC) carry sensory inputs (Cervantes-Sandoval et al., 2017; Tsao et al., 2018; Yagi et al., 2016) and those from DANs carry internal state information (Mao and Davis, 2009; Riemensperger et al., 2005; Zolin et al., 2021) to functional compartments of the MB, where dopamine release modulates the KC and MB output neuron synapse (MBONs; Aso et al. 2014). The KC-DAN-MBON tripartite synapse, carries a dynamically updating representation of the motivational and behavioural state of the animal (Aso and Rubin, 2016; Berry et al., 2015; Owald et al., 2015; Waddell, 2016). Here we have investigated the molecular mechanisms that underlie the ability of neuromodulatory acetylcholine signals, acting through SOCE during circuit maturation, to determine fpDAN function required for *Drosophila* flight.

Results

A spatio-temporal requirement for SOCE determines flight

97 To understand how neuromodulator stimulated SOCE alters neuronal
98 properties over developmental time scales we began by refining further the existing
99 spatio-temporal coordinates of SOCE requirement for flight. Flight promoting
100 dopaminergic neurons (DANs) with a requirement for SOCE have been identified
101 earlier by expression of a dominant negative *Orai* transgene, which renders the
102 channel Ca^{2+} impermeable, thus abrogating all SOCE as observed in primary neuronal
103 cultures (*Orai*^{E180A}; Figure 1A; Pathak et al. 2015; Yeromin et al. 2006). These include
104 a smaller subset of *THD'GAL4* marked DANs, where acetylcholine promotes
105 dopamine release through the muscarinic acetylcholine receptor (mAchR) by
106 stimulating IP_3/Ca^{2+} signaling (Sharma and Hasan, 2020). *Orai*^{E180A} expression in a
107 subset of 21-23 dopaminergic neurons marked by *THD' GAL4* (Figure 1B) led to
108 complete loss of flight (Figure 1C) while overexpression of the wildtype *Orai* transgene
109 had a relatively minor effect (Figure S1A).
110 *THD'* marks DANs in the PPL1, PPL2, and PPM3 clusters of the adult central
111 brain (Figure 1B) of which the PPL1 (10-12) and PPM3 (6-7) cell clusters constitute
112 the fpDANs (Pathak et al., 2015). Among these 16-19 DANs, two pairs of PPL1 DANs
113 projecting to the $\gamma 2\alpha'1$ lobes of the mushroom body (marked by the MB296B split
114 GAL4 driver and schematised in Figure S1B; Aso et al. 2014; Aso and Rubin 2016)
115 were identified as contributing to the flight deficit to a significant extent (Figures 1C;
116 S1C). The MB296B DANs form part of a central flight relay centre identified earlier as
117 requiring IP_3/Ca^{2+} signaling (Sharma and Hasan, 2020). That the *THD'* neurons are
118 required for flight was further confirmed by inhibiting their function. Acute activation of
119 either a temperature sensitive *Dynamin* mutant (*Shibire*^{ts}; Kitamoto 2001), which
120 blocks exocytosis at an elevated temperature, or acute expression of the tetanus toxin
121 light chain fragment (*TeTxLC* ; Sweeney et al. 1995) which cleaves *Synaptobrevin*, an
122 essential component of the synaptic release machinery in *THD'* neurons led to severe
123 flight defects (Figure S1D).
124 Previous work has demonstrated that intracellular Ca^{2+} release through the
125 IP_3R, that precedes SOCE (Figure 1A), is required during late pupal development in
126 *THD'* marked DANs for flight (Pathak et al., 2015; Sharma and Hasan, 2020). The
127 precise temporal requirement for SOCE in *THD'* neurons was investigated by inducing
128 *Orai*^{E180A} transgene expression for specific periods of pupal development and in adults

129 with the *tubulinGAL80^{ts}* based temperature sensitive expression system, (TARGET-
130 Temporal And Regional Gene Expression Targeting; McGuire et al., 2004).
131 Approximately 100 hours of pupal development were binned into 24 hour windows,
132 wherein SOCE was abrogated by *Orai^{E180A}* expression, following which, normal
133 development and growth was permitted. Flies were assayed for flight 5 days post
134 eclosion. Abrogation of SOCE by expression of the *Orai^{E180A}* dominant negative
135 transgene at 72 to 96 hrs after puparium formation (APF), resulted in complete loss of
136 flight as compared to minor flight deficits observed upon expression of *Orai^{E180A}* during
137 earlier developmental windows (Figure 1D). Abrogation of flight also occurred upon
138 *Orai^{E180A}* expression during the first 2 days post-eclosion (see discussion) whereas
139 abrogation of SOCE 5 days after eclosion as adults resulted in only modest flight
140 deficits (Figure 1D), indicating that SOCE is required for maturation of *THD'* marked
141 flight dopaminergic neurons. Earlier work has shown that loss of SOCE by expression
142 of *Orai^{E180A}* does not alter the number of dopaminergic neurons or affect neurite
143 projection patterns of PPL1 and PPM3 neurons (Pathak et al., 2015). Of these two
144 clusters, PPM3 DANs project to the ellipsoid body in the central complex (Kong et al.,
145 2010), and PPL1 DANs project to the mushroom body and the lateral horn (Mao and
146 Davis, 2009) and aid in the maintenance of extended flight bouts (Sharma and Hasan,
147 2020).
148
149 **Loss of SOCE in late pupae leads to a re-organisation of neuronal gene**
150 **expression**
151 The molecular consequences of loss of SOCE in *THD'* neurons were
152 investigated next by undertaking a comprehensive transcriptomic analysis from
153 fluorescence activated and sorted (FACS) *THD'* neurons with or without *Orai^{E180A}*
154 expression and marked with eGFP (Figure 1E; S1E). *THD'* neurons were obtained
155 from pupae at 72 ± 6h APF (essential SOCE requirement for flight; Figure 1E).
156 Expression analysis of RNAseq libraries generated from *THD'* neurons revealed a
157 reorganisation of the transcriptome upon loss of SOCE (Figure 1F). Expression of 822
158 genes was downregulated (with a fold change cut-off of < -1) as assessed using 3
159 different methods of Differentially Expressed Genes (DEG) analysis (Figure 1G)
160 whereas 137 genes were upregulated (Figure S1F). To understand if loss of SOCE

161 affects genes expressed in neurons from the pupal stage, we used the modEncode
162 dataset (Celniker et al., 2009; modENCODE Consortium et al., 2010) to reconstruct
163 developmental trajectories of all genes expressed in *THD'* neurons (Figure S1G).
164 Using an unsupervised clustering algorithm, we classified genes expressed in *THD'*
165 neurons into 3 clusters where 'Cluster 0' is low expression throughout development;
166 'Cluster 1' exhibits a larval peak in expression and 'Cluster 2' exhibits a pupal peak in
167 expression (Figure 1H). The majority of expressed genes (>95%) classify as low
168 expression throughout (Cluster 0) and were removed from further analysis. Genes
169 belonging to either the downregulated gene set or the upregulated gene set in SOCE-
170 deficient *THD'* neurons and a random set of genes were analysed further. A
171 comparison of the proportion of DEGs classified in the larval and pupal clusters
172 revealed that >75% of downregulated genes belonged to the pupal peak (Cluster 2)
173 whereas <20% of either the upregulated genes or a random set of genes classified as
174 belonging to the larval peak (Figure 1I). Moreover, downregulated genes exhibit higher
175 baseline expression in wildtype pupal *THD'* neurons (Figures S1H, I). These analyses
176 suggest that SOCE induces expression of a set of genes in *THD'* neurons during the
177 late pupal phase which are subsequently required for flight. These are henceforth
178 referred to as SOCE-responsive genes.
179
180 **SOCE regulates gene expression through a balance of Histone 3 Lysine 36**
181 **trimethylation and Histone 3 Lysine 27 trimethylation**
182 Gene ontology (GO) analysis of SOCE-responsive genes revealed
183 'Transcription', 'Ion transporters', 'Ca^{2+} dependent exocytosis', 'GPCRs', 'Synaptic
184 components', and 'Kinases' as top GO categories (Figure 2A). Among these,
185 'Transcription' and 'Ion transporters' represented categories with the highest
186 enrichment. Further analysis of genes that classified under 'Transcription' revealed
187 SET domain containing genes that encode histone lysine methyltransferases
188 implicated in chromatin regulation and gene expression (Dillon et al., 2005) and
189 among the SET domain containing genes, *Set1* and *Set2* showed distinct
190 downregulation (Figure 2B). One of these genes, the H3K36me3 methyltransferase
191 *Set2* (Figure 2C), was identified in a previous RNAseq from larval neurons with loss
192 of IP_3R-mediated Ca^{2+} signaling (Mitra et al., 2020). RT-PCRs from sorted *THD'*

193 neurons confirmed that *Set2* levels are indeed downregulated (by 76%) in *THD'*
194 neurons expressing *Orai*^{E180A} and to the same extent as seen upon expression of
195 *Set2*^{RNAi} (79% downregulation; Figure 2C). *Set1* and *Set2* perform methyltransferase
196 activity at H3K4 and H3K36 histone residues respectively (Ardehali et al., 2011;
197 Stabell et al., 2007). Both these markers are epigenetic signatures for transcriptional
198 activation, where H3K4me3 is enriched at the 5' end of the gene body and H3K36me3
199 is enriched in the gene bodies of actively transcribed genes ; schematised in Figure
200 S2A). In the adult CNS, *Set2*, is expressed at 4-fold higher levels compared to *Set1*
201 (Figure S2B; modENCODE Consortium et al., 2010). *Set2* also shows a steep 5.5 fold
202 increase in expression levels during the pupal to adult transition, compared to a 2 fold
203 increase in *Set1* (Figure S2B). These observations coupled with the previous report of
204 Set2 function downstream of IP_3R/Ca^{2+} signaling in larval glutamatergic neurons (Mitra
205 et al., 2020), led us to pursue the role of Set2 in *THD'* neurons.
206 *Set2* encodes the only *Drosophila* methyltransferase which is specific for
207 H3K36 trimethylation (Stabell et al., 2007). To understand the functional significance,
208 if any, of down-regulation of *Set2* in *THD'* neurons upon loss of SOCE, four
209 independent *Set2* RNAi constructs were obtained. Knockdown of *Set2* in *THD'*
210 neurons with all four RNAi lines tested resulted in significant flight defects (Figure 2D;
211 S2C). *Set2* function for flight was additionally verified in the PPL1 DANs projecting to
212 the $\gamma 2\alpha'1$ lobe of the mushroom body (*MB296BGAL4*; Figure S2D). To test the
213 hypothesis that *Set2* expression and function for flight is regulated by SOCE, we
214 overexpressed *Set2* in the *Orai*^{E180A} background, using GAL4-UAS driven
215 heterologous *Set2*^{WT} expression or CRISPR-dCas9::VPR driven overexpression
216 (Gilbert et al., 2013) from the endogenous locus, and measured flight (Figure 2D data
217 in purple and brown). Flies expressing *Orai*^{E180A} in the *THD'* neurons, which are
218 flightless, exhibit significant rescue in flight bout durations upon *Set2* overexpression,
219 through either method (Figure 2D, compare red with purple and brown data), but not
220 upon expression of a control transgene, *GCamP6m* (Figure S2E, compare data in
221 green and red). Although the *Set2* overexpression rescues were induced all through
222 development, because Orai function drives critical gene expression during 72-96 hrs
223 APF (Figure 1D), we concluded that Set2-mediated rescue is also likely to occur during
224 this time window. Furthermore, overexpression of a key SOCE component, the ER

225 Ca^{2+} sensor *STIM* in a *Set2*^{RNAi} background led to a rescue (Figure S2E, compare
226 pink and grey data). The rationale for attempting rescue of *Set2*^{RNAi} deficits by *STIM*
227 overexpression is based on previous results (Agrawal et al., 2010; Chakraborty et al.,
228 2016; Deb et al., 2016), where impaired IP_3R function and reduced SOCE, could be
229 restored to a significant extent in primary neuronal cultures, followed by rescue of flight
230 initiation in flies of the same genotypes, upon *STIM* overexpression. *STIM*^{OE} in the
231 *Set2*^{RNAi} background is thus expected to enhance SOCE, which we predict would
232 rescue *Set2* expression leading to the rescue of other Set2 dependent phenotypes
233 like flight. These two sets of data taken together with downregulation of *Set2* upon
234 expression of *Orai*^{E180A} (Figure 2C) support the hypothesis that SOCE driven
235 expression of *Set2* in fpDANs is required for flight. That Set2 function downstream of
236 SOCE, occurs specifically through its methyltransferase activity was supported
237 through experiments where knockdown of the demethylase *Kdm4B*, the primary
238 histone demethylase expressed in these neurons (Figure S2F), rescued flight in
239 *THD'>Orai*^{E180A} flies (Figure 2D; data in pink). Knockdown of the lower expressed
240 *Drosophila* H3K36 demethylase isoform, *Kdm4A,* did not show a similar rescue
241 (Figure S2G; data in pink). Moreover, both *Set2* depletion and loss of SOCE
242 (*THD'>Orai*^{E180A}) lead to a decrease in the normalised H3K36me3 signal in *THD'*
243 neurons (Figure 2E).

244 To understand if deficient H3K36me3 is found in the SOCE-responsive genes,
245 we quantified the enrichment of H3K36me3 at SOCE-responsive loci from an
246 H3K36me3 ChIP-Seq dataset (modENCODE Consortium et al., 2010) from wild-type
247 adult heads (Figure 2F). We observed an enrichment of the H3K36me3 signal over
248 the gene bodies of the SOCE-responsive genes (Figure 2F). Additionally, genes that
249 were more affected by loss of SOCE (greater extent of downregulation), had a
250 correspondingly higher H3K36me3 signal (Figure 2G) as compared with a random set
251 of genes (Figure 2G; data in grey), further indicating that one of the ways SOCE
252 regulates gene expression is through Set2 mediated deposition of H3K36me3.

253 The gene *E(z)* that encodes a component of the PRC2 complex (*EZH2*), which
254 deposits H3K27me3 is up-regulated upon loss of SOCE (Figure 2B) suggesting that
255 SOCE could affect additional histone modifications. While H3K36me3 is a marker for
256 transcriptional activation (Krogan et al., 2003), H3K27me3 is a repressive signature

257 which silences transcription (Cai et al., 2021). These two marks are antagonistic as
258 deduced from studies which have shown that deposition of H3K36me3 allosterically
259 inhibits the Polycomb Repressive Complex (PRC2), thereby preventing it from
260 depositing the H3K27me3 signature at the same genomic loci (Finogenova et al.,
261 2020). A comparison of H3K36me3 and H3K27me3 peaks over the 822 SOCE-
262 responsive genes revealed a higher enrichment of H3K36me3 versus H3K27me3 in
263 wild type fly heads (Figure 2H; modENCODE Consortium et al., 2010), suggesting that
264 robust expression of these genes in adult neurons occurs through a SOCE-dependent
265 mechanism initiated in late pupae (schematised in Figure 2I). To test this hypothesis,
266 we fed SOCE-deficient flies (*THD'GAL4>Orai*^{E180A}) GSK343, a pharmacological
267 inhibitor (Verma et al., 2012) of the EZH2 component of PRC2 that is known to reduce
268 H3K27me3 chromatin marks and performed flight assays. Feeding of GSK343 lead to
269 partial rescue of flight in *THD'> Orai*^{E180A} flies in a dose dependent manner with
270 maximal flight bout durations of up to 400 sec (Figure 2J; S2H).
271

272 **Normal cellular responses of PPL1 DANs require Orai mediated SOCE and**
273 **H3K36 trimethylation**

274 Next we investigated Ca^{2+} responses in SOCE and H3K36 trimethylation
275 deficient *THD'* PPL1 DANs upon stimulation with a neuromodulatory signal for the
276 muscarinic acetylcholine receptor (mAChR). It is known that *THD'* marked PPL1 DANs
277 receive cholinergic inputs that stimulate store Ca^{2+} release through the IP_3R, leading
278 to SOCE through Orai (Figure 3A; Ebihara et al., 2006; Sharma and Hasan, 2020). In
279 support of this idea, either expression of *Orai*^{E180A} or knockdown of the IP_3R attenuated
280 the response to carbachol (CCh), a mAChR agonist, in PPL1 DANs (Figure 3B-D;
281 Figure S3A-C). Importantly, knockdown of *Set2* also abrogated the Ca^{2+} response to
282 CCh (Figure 3B-D), whereas overexpression of a transgene encoding *Set2* in *THD'*
283 neurons either with loss of SOCE (*Orai*^{E180A}) or with knockdown of the IP_3R (*itpr*^{RNAi}),
284 lead to significant rescue of the Ca^{2+} response, indicating that *Set2* is required
285 downstream of SOCE (Figure 3B-D) and IP_3/Ca^{2+} signalling (Figure S3A-C).

286 An understanding of how Set2 might rescue cellular IP_3/Ca^{2+} signaling was
287 obtained in an earlier study where it was demonstrated that *Set2* participates in a
288 transcriptional feedback loop to control the expression of key upstream components

289 such as the *mAChR* and the *IP$_3$R* in a set of larval glutamatergic neurons (Mitra et al.,
290 2021). To test whether *Set2* acts through a similar transcriptional feedback loop in the
291 current context, *THD'* DANs were isolated using FACS from appropriate genetic
292 backgrounds and tested for expression of key genes required for IP$_3$/Ca^{2+} signaling
293 (*mAChR* and *itpr)* and SOCE (*Stim* and *Orai*). Loss of SOCE upon expression of
294 *Orai^{E180A}* lead to a significant decrease in the expression of *itpr (72%* downregulation;
295 Figure 3E*)*, *mAChR (56%* downregulation; Figure 3E*)*, *Stim (63%* downregulation;
296 Figure 3E) in *THD'* DANs. As expected *Orai* expression (Figure 3E) increased 2-fold
297 presumably due to overexpression of the *Orai^{E180A}* transgene. Importantly, knockdown
298 of *Set2* in *THD'* neurons also led to downregulation of *itpr* (43%), *mAChR* (78%) and
299 *Stim* (61%) (Figure 3E). Overexpression of *Set2* in the background of *Orai^{E180A}* led to
300 a rescue in the levels of *itpr* (69% increase), *mAChR* (43% increase), and *Stim* (40%
301 increase) (Figure 3E). Overexpression of *Set2* in wildtype *THD'* neurons resulted in
302 upregulation of *mAChR* and *Orai* (Figure 3E). These findings indicate that while SOCE
303 regulates *Set2* expression (Figure 2C), *Set2* in turn functions in a feedback loop to
304 regulate expression of key components of IP$_3$/Ca^{2+} (*mAchR* and *IP$_3$R*) and SOCE
305 *(STIM* and *Orai)* (Figure 3E). Thus, ectopic *Set2* overexpression in SOCE deficient
306 *THD'* neurons, leads to increase in expression of key genes that facilitate intracellular
307 Ca^{2+} signalling and SOCE (schematised in Figure 3F). Direct measures of Orai-
308 channel function under conditions of altered *Set2* expression are needed in future to
309 assess how the feed-back loop alters carbachol-induced ER-Ca^{2+} release and SOCE
310 independent of each other (see 'Limitations of this study' in discussion). While we
311 assume that the observed changes in gene expression translate to alterations in
312 protein levels, direct measurement of protein levels specifically from *THD'* neurons
313 need to be addressed in future.
314

315 **Trithorax-like or Trl is an SOCE responsive transcription factor in *THD'* DANs**

316 The data so far identify SOCE as a key developmental regulator of the neuronal
317 transcriptome in *THD'* marked DANs, where it upregulates *Set2* expression and thus
318 enhances the activation mark of H3K36 trimethylation on specific chromatin regions.
319 However, the mechanism by which SOCE regulates expression of *Set2,* and other
320 relevant effector genes remained unresolved (Figure 3F). In mammalian T cells,

321 SOCE leads to de-phosphorylation of the NFAT (Nuclear Factor of Activated T-cells)
322 family of transcription factors by Ca^{2+}/Calmodulin sensitive phosphatase Calcineurin,
323 followed by their nuclear translocation and ultimately transcription of relevant target
324 genes (Hogan et al., 2003). Unlike mammals, the *Drosophila* genome encodes a
325 single member of the NFAT gene family, which does not possess calcineurin binding
326 sites, and is therefore insensitive to intracellular Ca^{2+} and SOCE (Keyser et al., 2007).
327 In order to identify transcription factors (TFs) that regulate SOCE-mediated
328 gene expression in *Drosophila* neurons, we examined the upstream regions (up to 10
329 kb) of SOCE-regulated genes using motif enrichment analysis (Zambelli et al., 2009)
330 for TF binding sites (Figure 4A). This analysis helped identify several putative TFs with
331 enriched binding sites in the regulatory regions of SOCE-regulated genes (Figure 4B,
332 S4A) which were then analyzed for developmental expression trajectories (Hu et al.,
333 2017) in the *Drosophila* CNS (Figure 4B; lower panel). Among the top 10 identified
334 TFs, the homeobox transcription factor Trl/GAF had the highest enrichment value,
335 lowest p-value (Figure 4B) and was consistently expressed in the CNS through all
336 developmental stages, with a distinct peak during pupal development (Figure 4B;
337 lower panel). To test the functional significance of Trl/GAF, we tested flight in flies with
338 *THD'* specific knockdown of *Trl* using two independent RNAi lines (Figure 4C) as well
339 as in existing *Trl* mutant combinations that were viable as adults (Figure S4B). While
340 homozygous *trl* null alleles are lethal, trans-heterozygotes of two different
341 hypomorphic alleles were viable and exhibit significant flight deficits (Figure 4C, S4B).
342 Moreover, the flight deficits caused by Trl^{RNAi} specifically in the *THD'* neurons could
343 be rescued by raising SOCE either directly through overexpression of *STIM* or
344 indirectly by *Set2* overexpression (Figure 4C; data in brown and pink respectively).
345 To further test Trl function, as an effector of intracellular Ca^{2+} signaling and
346 SOCE, we investigated genetic interactions of $trl^{13C,}$ a hypomorphic mutant recessive
347 *Trl* allele, with an existing deficiency for the ER-Ca^{2+} sensor STIM ($STIM^{KO}$), an
348 essential activator of the Orai channel (Wang et al., 2010) as well as existing mutants
349 for an intracellular ER-Ca^{2+} release channel, the IP_3R (Joshi et al., 2004). While
350 $STIM^{KO}/+$ flies demonstrate normal flight bout durations, adding a single copy of the
351 trl^{13C} allele to the $STIM^{KO}$ heterozygotes ($STIM^{KO}/+;\ trl^{13C}/+$ trans-heterozygotes)
352 resulted in significant flight deficits, which could be rescued by overexpression of either

353 *STIM* or *Set2* (Figure 4D). The rescue of *STIM*^{KO}/+; *trl*^{13C}/+ with *STIM*^{OE} (Figure 4D)
354 indicates that SOCE, driven by *STIM*^{OE}, activates residual Trl encoded by a copy of
355 *Trl*$^{+}$ in this genetic background (*trl*^{13c}/+) to rescue flight. The role of Trl as an SOCE-
356 regulated transcription factor is further supported by rescue of flight in *STIM*^{KO}/+;
357 *trl13c*/+ flies by overexpression of *Set2* (Figure 4D). Set2 expression in *THD'* neurons
358 was demonstrated earlier as requiring Orai mediated Ca^{2+} entry (Figure 2B-C). These
359 genetic data are consistent with the positive feedback loop proposed earlier (Figure
360 3F). We hypothesize that Trl is non-functional upon expression of *Orai*^{E180A} due to
361 reduced SOCE. Loss of Trl function in turn down-regulates *Set2* expression. A single
362 copy of *trl*^{13C} placed in combination with a single copy of various *itpr* mutant alleles,
363 also showed a significant reduction in the duration of flight bouts (Figure S4C), further
364 supporting a role for intracellular Ca^{2+} signaling in Trl function. Flight deficits observed
365 upon specific expression of *Trl*^{RNAi} in *THD'* neurons (Figure 4C) indicate the direct
366 requirement of Trl in fpDANs. Taken together, these findings provide good genetic
367 evidence for Trl as a SOCE-responsive TF in *THD'* neurons. Due to the strong flight
368 deficit observed by expression of *Orai*^{E180A} we were unable to test genetic interactions
369 of *Trl* with Orai directly. *Orai*^{RNAi} strains exhibit off-target effects and *Orai* hypomorphs
370 are unavailable.

371 The requirement of *Trl* for SOCE-dependent gene expression was tested
372 directly by measuring *Set2* transcripts in FACS sorted *THD'* neurons with knockdown
373 of *Trl* (*THD'>Trl*^{RNAi}). *Set2* has 20 Trl binding sites in a 2 Kb region upstream of the
374 transcription start site (Figure S4D) and knockdown of *Trl* resulted in downregulation
375 of *Set2* (32%) and the Set2 regulated genes *itpr* (56%) and *mAchR* (73%; Figure 4E).
376 Moreover, a trans-heterozygotic combination of hypomorphic Trl alleles (*trl*$^{13C/62}$) had
377 markedly reduced levels of brain H3K36me3 (Figure 4F).

378 To test if Trl drives cellular function in the fpDANs, we stimulated the mAChR
379 with CCh and measured Ca^{2+} responses in fpDANs with knockdown of *Trl*. Compared
380 to *WT* fpDANs, which respond robustly to cholinergic stimulation, *Trl*^{RNAi} expressing
381 DANs, exhibit strongly attenuated responses (Figure 4G-I). Overexpression of *Set2* in
382 the *Trl*^{RNAi} background rescued the cholinergic response (Figure 4G-I). The rescue of
383 both flight (Figure 4C, D) and the cholinergic response (Figure 4G-I) by overexpression

384 of *Set2* in flies with knockdown of *Trl* in *THD'* neurons (*THD'>Trl*^{RNAi}), confirms that Trl
385 acts upstream of *Set2* to ensure optimal neuronal function and flight.
386
387 The results obtained so far indicate that Trl functions as an intermediary
388 transcription factor between SOCE and its downstream effector gene *Set2*.
389 Overexpression of *Trl*, however, is unable to rescue the loss of flight caused by loss
390 of SOCE (*THD'>Orai*^{E180A}; Figure 5A). Moreover, *Trl* transcript levels are unchanged
391 in the *Orai*^{E180A} condition (Figure 5B). These data could either mean that phenotypes
392 observed upon loss of Trl are independent of Orai-Ca^{2+} entry or that Trl requires Ca^{2+}
393 influx through SOCE for its function to go from an 'inactive' form to an 'active' form
394 (schematized in Figure 5C). We favor the latter interpretation because key transcripts
395 downregulated by expression of *Orai*^{E180A} (*Set2, itpr* and *mAchR*) were also
396 downregulated upon knockdown of *Trl* in *THD'* neurons (see Figures 3E and 4E).
397 To understand how Orai-mediated Ca^{2+} entry might activate Trl we went back
398 to previously known biochemical characterization of Trl. Although Trl does not possess
399 a defined Ca^{2+} binding domain, it interacts with a diverse set of proteins, primarily
400 through its BTB-POZ domain (Figure S5A) as demonstrated earlier by affinity
401 purification of Trl from embryonic extracts followed by high throughput mass
402 spectrometry (Lomaev et al., 2017). Among the identified interacting partners, we
403 focused on kinases, keeping in mind an earlier study in *Drosophila* indicating
404 phosphorylation of Trl at a threonine residue (T237; Zhai et al., 2008). Analysis of the
405 Trl interactome revealed several kinases, which were expressed to varying extents in
406 the *THD'* neurons (Figure S5B), including the Ca^{2+} dependent CamKII, implicated
407 earlier in flight in *THD'* neurons (Ravi and Hasan 2018). Loss of CamKII in *THD'*
408 neurons by RNAi mediated knockdown or through expression of a peptide inhibitor
409 (Ala; Mehren and Griffith, 2004) resulted in significant flight deficits (Figure S5C). To
410 test if CamKII activation downstream of SOCE is required for flight, we expressed a
411 constitutively active version of CamKII (*T287D*; Kadas et al., 2012) in the background
412 of *THD'>Orai*^{E180A}. The phosphomimetic *CamKII*^{T287D} point mutation renders CamKII
413 activity Ca^{2+} independent (Malik and Hodge, 2014). Acute expression of *CamKII*^{T287D}
414 in the *Orai*^{E180A} background using the TARGET system (McGuire et al., 2004) resulted
415 in a weak rescue of flight when implemented from 72 to 96 hrs APF (Figure S5D)

416 whereas overexpression of WT *CamKII* or a phosphorylation-incompetent allele
417 (*CamKII*^{T287A}), failed to rescue flight (Figure S5D). These data support a model
418 (schematized in Figure 5C) wherein Ca^{2+} influx through SOCE sustains Trl activation,
419 in part through CamKII, leading to expression of *Set2* followed by increased levels of
420 chromatin H3K36me3 marks that drive further downstream gene expression changes
421 through a transcriptional feedback loop. Our data do not rule out activation of other
422 Ca^{2+} sensitive mechanisms for activation of Trl. Moreover, rescue of flight in Trl
423 mutant/knockdown conditions by *STIM* overexpression (Figure 4C and 4D) suggests
424 the presence of additional SOCE-responsive transcription factors in fpDANs.
425

426 **Trl function downstream of SOCE targets neuronal activity through changes in**
427 **ion channel gene expression including VGCCs**

428 Next we investigated the extent to which the identified SOCE-Trl-Set2
429 mechanism impacts fpDAN function. 'Ion transport' is among the top GO terms
430 identified in SOCE-responsive genes (Figure 2A). Indeed, multiple classes of ion
431 channel genes including several $Na^{+,}$ K^{+} and Cl^{-} channels are downregulated in
432 fpDANs upon expression of *Orai*^{E180A} (Fig 5D, E). Regulation of ion channel gene
433 expression by Trl was indicated from the enrichment of Trl binding sites in regulatory
434 regions of some ion channel loci (Figure 5F). We purified fpDANs with knock down of
435 *Trl* (*THD'>Trl*$^{RNAi-1}$) and measured expression of a few key voltage-gated ion channel
436 genes (Fig 5F). *NaCP60E*, *para* (Na^{+} channels), *cac*, *ca-α1D* (VGCC subunits), *hk*,
437 and *eag* (outward rectifying K^{+} channels) are all downregulated between 0.6-0.9 fold
438 upon *Trl* knockdown (Fig 5G) as well as upon loss of SOCE (Fig 5B). Taken together,
439 these results indicate that the expression of key voltage-gated ion channel genes
440 which are required for the depolarization-mediated response, maintenance of
441 electrical excitability and neurotransmitter release is a focus of the transcriptional
442 program set in place by SOCE-Trl-Set2 .

443 To test the functional consequences of altered ion channel gene expression
444 downstream of Trl, neuronal activity of the fpDANs was tested by means of KCl-
445 evoked depolarisation. PPL1 DANs exhibited a robust Ca^{2+} response that was lost
446 upon knock down of *Trl* (Figure 5H-J; data in orange). In consonance with the earlier
447 behavioural experiments (Figure 5A), overexpression of *Trl*$^{+}$ in *THD'* DANs did not

448 rescue the KCl response in PPL1 DANs with loss of SOCE (*OraiE*^{180A}*; Trl*^{OE}, Figure
449 5I, J), further reinforcing the hypothesis that, Trl activity in fpDANs is dependent of
450 Ca^{2+} entry through Orai.

451 Response to KCl is also lost in PPL1 neurons by knockdown of *Set2* and
452 restored to a significant extent by overexpression of *Set2* in *THD'* DANs lacking SOCE
453 (*Orai*^{E180A}*;Set2*$^{OE;}$ Figure 6A-C). We confirmed that the KCl response of PPL1 neurons
454 requires VGCC function, either by treatment with Nimodopine (Xu and Lipscombe,
455 2001), an L-type VGCC inhibitor or by knockdown of a conserved VGCC subunit *cac*
456 *(cac*^{RNAi}*)*. Both forms of perturbation abrogated the depolarisation response to KCl in
457 PPL1 neurons (Figures 6D-F; data in purple or orange respectively). Moreover, the
458 Ca^{2+} entry upon KCl-mediated depolarization in PPL1 neurons is a cell-autonomous
459 property as evident by measuring the response after treatment with the Na^{+} channel
460 inhibitor, Tetrodotoxin (TTX; Figures 6D-F; data in magenta).

461 Having confirmed that the Ca^{2+} response towards KCl depolarisation requires
462 VGCCs, we tested the expression level of key components of *Drosophila* VGCCs
463 (Figure 6G) in *THD'* DANs, including *cacophony* (*cac*), *ca-α1D*, *ca-α1T*, and *ca-β*. All
464 four subunits of *Drosophila* VGCC are downregulated upon loss of SOCE (*Orai*^{E180A};
465 Figure 6H) in *THD*' DANs whereas overexpression of *Set2* in the background of
466 *Orai*^{E180A} restored expression of the four VGCC subunits tested (Figure 6H), thus
467 explaining recovery of the KCl response upon *Set2* overexpression in PPL1 neurons
468 lacking SOCE (*Orai*^{E180A}; Figures 6A-C).

469 The functional significance of downregulation of VGCC subunits by the SOCE-
470 Trl-Set2 pathway was tested directly by knockdown of the 4 VGCC subunits
471 independently in PPL1 neurons followed by measurement of flight bout durations.
472 Significant loss of flight was observed with knockdown of each subunit (Figure 6I)
473 though in no case was the phenotype as strong as what is observed with loss of SOCE
474 (*Orai*^{E180A}; Figure 1D). These data suggest that in addition to VGCC subunit
475 expression, appropriate expression of other ion channels in the fpDANs is of functional
476 significance. This idea is further supported by the observation that loss of flight upon
477 loss of SOCE cannot be restored by overexpression of *cac* alone (Figure 6J)
478 indicating that optimal neuronal activity requires an ensemble of genes, including ion
479 channels, whose expression is regulated by SOCE-Trl-Set2.

480

481 ***THD'* DANs require SOCE for developmental maturation of neuronal activity**

482 The functional relevance of changes in neuronal activity during pupal
483 maturation of the PPL1-dependent flight circuit was tested next. Inhibition of *THD'*
484 DANs from 72 to 96 hours APF using acute induction of the inward rectifying K^+
485 channel *Kir2.1*(Johns et al., 1999) or optogenetic inhibition through the hyperpolarizing
486 Cl^- channel *GtACR2* (Govorunova et al., 2015) resulted in significant flight deficits
487 (Figure 7A; data in dark or light green). Similar flight defects were recapitulated upon
488 hyperactivation of *THD'* neurons through either optogenetic (*CsChrimson*; Klapoetke
489 et al., 2014) or thermogenetic (*TrpA1*; Viswanath et al., 2003) stimulation (Figure 7A;
490 data in orange or red), indicating that these neurons require balanced neuronal activity
491 during a critical window in late pupal development, failing which the flight circuit
492 malfunctions. To test if restoring excitability in fpDANs lacking SOCE *(THD'>Orai^{E180A}*)
493 is sufficient to restore flight, we induced hyperexcitability by overexpressing *NachBac*
494 (Nitabach, 2006) a bacterial Na^+ channel. *NachBac* expression rescued both flight
495 (*THD'>Orai^{E180A}*; Figure 7B) and excitability (Figures 7C-E). A partial rescue of flight
496 was also obtained by optogenetic stimulation of neuronal activity through activation of
497 *THD'>Orai^{E180A}* DANs using *CsChrimson* either 72-79 hrs APF or 0-2 days post
498 eclosion (Figure 7E). In this case, flight rescues were accompanied by a
499 corresponding rescue of *CsChrimson* activation induced Ca^{2+} entry (Figures 7F, G).
500 Moreover inducing neuronal hyperactivation with indirect methods such as excess K^+
501 supplementation (Figure S7A) or impeding glial K^+ uptake, by genetic depletion of the
502 glial K^+ channel *sandman* (Weiss et al., 2019), partially rescued flight in animals
503 lacking SOCE in the *THD'* DANs (Figure S7B). Together, these results indicate that
504 SOCE, through Trl and Set2 activity, determines activity in fpDAN during circuit
505 maturation by regulating expression of voltage-gated ion channel genes, like *cac* (see
506 discussion).

507 fpDANs also require a balance between H3K36me3/H3K27me3 mediated
508 epigenetic regulation (Figure 2K). To understand if this epigenetic balance affects
509 flight through modulation of neuronal excitability, we measured KCl-induced
510 depolarizing responses of PPL1 DANs in Orai deficient animals (*THD'>Orai^{E180A}*) fed
511 on the H3K27me3 antagonist GSK343 (0.5 mM). GSK343 fed animals were sorted

512 into 2 groups (Fliers/Non-Fliers) on the basis of flight bout durations of greater or lesser
513 than 30 s (Figure S7C), and tested for responses to KCl (Figures S7D, E).
514 *THD'>Orai*^{E180A} flies fed on GSK343 showed a rescue in KCl responses, with a clearly
515 enhanced response in the fliers compared to the non-fliers (Figures S7D, E), thereby
516 reiterating the hypothesis that SOCE-mediated regulation of activity in these neurons
517 acts through epigenetic regulation between opposing histone modifications.
518

519 ***THD'* DANs require SOCE-mediated gene expression for axonal arborization and**
520 **neuromodulatory dopamine release in the mushroom body γ lobe**

521 Next, we re-visited how loss of activity during the critical maturation window of
522 72-96 hrs APF and 0-2 days post-eclosion affects axonal arborisation of fpDANs that
523 innervate the γ lobe. From previous work we know that major axonal branches of the
524 fpDANs reach the γ lobe normally in *THD'>Orai*^{E180A} animals (Figure 8A, B; Pathak et
525 al., 2015). Neuronal activity can drive changes in neurite complexity and axonal
526 arborization (Depetris-Chauvin et al., 2011) especially during critical developmental
527 periods (Sachse et al., 2007). To understand if Orai mediated Ca^{2+} entry and
528 downstream gene expression through Set2 affects this activity-driven parameter, we
529 investigated the complexity of fpDAN presynaptic terminals within the γ2α'1 lobe MB
530 using super-resolution microscopy (Figure 8 A, B). Striking changes in the neurite
531 volume upon expression of *Orai*^{E180A} were observed. Importantly these changes could
532 be rescued to a significant extent by restoring either *Set2* (*Orai*^{E180A}*; Set2*^{OE}) or by
533 inducing hyperactivity through *NachBac* expression (*Orai*^{E180A} *; NachBac*^{OE}; Figure 8
534 C, D).

535 To understand if reduced axonal arborisation within the γ lobe has functional
536 consequences we measured CCh-evoked DA release at the γ2α'1 region of the
537 mushroom body (Figure 8A; red arrow). For this purpose we used the dopamine
538 sensor *GRAB-DA* (Sun et al., 2018). Loss of SOCE (*THD'>Orai*^{E180A}) attenuated DA
539 release (Figures 8E, F, G), which could be partially rescued by overexpression of *Set2*.
540 Taken together these data identify an SOCE-dependent gene regulation mechanism
541 acting through the transcription factor Trl, and the histone modifier Set2 for timely
542 expression of genes that impact diverse aspects of neuronal function including

543 neuronal activity, axonal arborisation, and sustained neurotransmitter release
544 (schematised in Figure 8H).
545
546 **Discussion**
547 Over the course of development, neurons define an excitability set point within
548 a dynamic range (Truszkowski and Aizenman, 2015), which stabilizes existing
549 connections (Mayseless et al., 2023) and enables circuit maturation (Johnson-
550 Venkatesh et al., 2015). The setting of this threshold for individual classes of neurons
551 is based on the relative expression of various ion channels. In this study, we identify
552 an essential role for the store-operated Ca^{2+} channel *Orai* in determining ion channel
553 expression and neuronal activity in a subset of dopaminergic neurons central to a MB
554 circuit for *Drosophila* flight. Orai-mediated Ca^{2+} entry, initiated by neuromodulatory
555 acetylcholine signals, is required for amplification of a signalling cascade, that begins
556 by activation of the homeo-box transcription factor Trl, followed by upregulation of
557 several genes, including *Set2*, a gene that encodes an enzyme for an activating
558 epigenetic mark, H3K36me3. Set2 in turn establishes a transcriptional feedback loop
559 to drive expression of key neuronal signaling genes, including a repertoire of voltage-
560 gated ion channel genes required for neuronal activity in mature PPL1 dopaminergic
561 neurons.
562
563 **SOCE supports gene expression transitions during critical developmental**
564 **windows**
565 Studies in the *Drosophila* mushroom body have identified spontaneous bouts
566 of voltage-gated Ca^{2+} channel mediated neuronal activity, through as yet unknown
567 mechanisms, which occur during early adulthood driving refinement and maturation of
568 behaviours such as associative learning (Leinwand and Scott, 2021). Our studies
569 here, on a subset of 21-23 central dopaminergic neurons (Figures 1B, C) of which
570 some send projections to the mushroom body and regulate flight behaviour, provide a
571 mechanistic explanation for neuromodulation-dependent intracellular signaling
572 culminating in transcriptional maturation of a circuit supporting adult flight. In the critical
573 developmental window of 72-96 hrs APF, a cohort of SOCE-responsive genes, that
574 include a range of ion channels, undergo a wave of induction. Loss of SOCE at this

575 stage thus renders these neurons functionally incompetent (Figures 3B-D, 6G-I, 7D-
576 F) and abrogates flight (Figure 1D). Developmentally assembled neuronal circuits
577 require experience/activity-dependent maturation (Akin and Zipursky, 2020). The
578 requirement of SOCE for flight circuit function during the early post eclosion phase (0-
579 2 days) suggests that maturation of the flight circuit extends into early adulthood,
580 where presumably feedback from circuit activity may further refine synaptic strengths
581 (Sugie et al., 2018). Expression of *Orai*^{E180A} in 5 day old adults had no effect on flight
582 (Figure 1E), indicating that either SOCE is not required for maintaining gene
583 expression in adults or that wildtype Orai channel proteins from late pupal and early
584 adults perdure for long periods extending into adulthood. Loss of SOCE in adult brains
585 beyond 5-7 days, when Orai protein turnover might be expected, has not been
586 assessed so far. The absence of any visible changes to primary neurite patterning
587 suggests that SOCE in the MB-DANs works primarily to refine synaptic function at pre-
588 synaptic terminals within the MB lobe. Taken together, our findings, indicate an
589 important role for SOCE in restructuring the neuronal transcriptome during a critical
590 developmental transition, which facilitates key changes in neuronal function required
591 for circuit formation and adult behavior. In summary, our findings here identify Orai-
592 driven Ca^{2+} entry as a key signaling step for driving coordinated gene expression
593 enabling the maturation of nascent neuronal circuits and sustenance of adult
594 behaviour.
595
596 **SOCE regulates a balance between competing epigenetic signatures**
597 Chromatin structure and function is dynamic over the course of brain
598 development (Kishi and Gotoh, 2018). One way neurons achieve dynamic spatio-
599 temporal control over developmental gene expression is via epigenetic mechanisms
600 such as post translational histone modifications (Geng et al., 2021). Cells possess an
601 extensive toolkit of histone modifiers, with characterised effects on transcriptional
602 output by either activating or repressing gene expression (Bannister and Kouzarides,
603 2011). However, relatively little, is known about how modifiers of histone marks are in
604 turn regulated to bring about the requisite changes in neuronal gene expression over
605 developmental timescales.

606 The SET-domain containing family of histone modifiers (Figure 2B), including
607 H3K36me3 methyltransferase Set2 (Figure 2C), identified here appear to function as
608 key transcriptional effectors induced downstream of neuromodulatory inputs that
609 stimulate Store-operated Ca^{2+} entry through Orai during pupal and adult maturation of
610 flight promoting dopaminergic neurons. SOCE-driven *Set2*-mediated H3K36me3
611 enhances the expression of key GPCRS, components of intracellular Ca^{2+} signaling
612 (Figure 2A) and ion channels (Figures 6A, B) for optimal dopaminergic neuron function
613 (Figure 7D-F) and flight (Figure 1C). Rescue of flight by genetic depletion of an
614 epigenetic 'eraser' *Kdm4B*, an H3K36me3 demethylase (Figure 2D) suggests that a
615 balance between perdurance of H3K36me3 and its removal is actively maintained on
616 the expressed genes. Interestingly, another member of the SET domain family, *E(z)*
617 is up-regulated upon loss of SOCE (Figure 2B). *E(z)* is a component of the *Drosophila*
618 PRC2 complex (Polycomb repressive complex), which represses gene expression
619 through H2K27me3 (Margueron and Reinberg, 2011). Structural studies on
620 *Drosophila* nucleosomes have elucidated that the H3K36me3 modification
621 allosterically inhibits the PRC2 complex activity (Finogenova et al., 2020). Our findings
622 support a model wherein at key developmental stages, SOCE determines the level of
623 these competing epigenetic signatures thus allowing gene expression by enhancing
624 Set2 mediated H3K36me3 (Fig 2H). Loss of SOCE leads to deficient Set2-mediated
625 H3K36me3 (Figure 2E), a likely shifting of the balance in favour of PRC2 mediated
626 H3K27me3 and overall repression in gene expression (as observed in Fig S1H, I).
627 Feeding SOCE-deficient animals a pharmacological inhibitor of PRC2 (GSK434) led
628 to a significant rescue in behaviour (Figure 2J) presumably by disinhibition of
629 H3K27me3 mediated gene repression. Though flight initiation is rescued in a dose
630 dependent manner, the duration of flight bouts is not sustained (Figure S2H) indicating
631 that suppression of H3K27me3 marks in the SOCE-deficient flies is partial. These
632 findings indicate additional roles for other histone modifications such as Set1 mediated
633 H3K4me3, which may work in concert to regulate developmental gene expression
634 programs stimulated by SOCE. Future studies directed at a comprehensive
635 cataloguing of multiple epigenetic signatures in defined neuronal subsets using cell-
636 specific techniques should help elucidate these mechanisms.
637

638 **Trl as an SOCE responsive transcription factor**

639 SOCE-mediated regulation of gene expression has been reported in
640 mammalian neural progenitor cells (Somasundaram et al., 2014) and *Drosophila* pupal
641 neurons (Pathak et al., 2015; Richhariya et al., 2017), through as yet unknown
642 mechanisms. A combination of motif enrichment analysis over regulatory regions of
643 SOCE-responsive genes and expression enrichment analysis in cells of interest,
644 helped generate a list of putative SOCE-responsive transcription factors (Figure 4A,
645 B). Among these we experimentally validated Trl/Trithorax-like/GAGA factor (GAF) as
646 a transcription factor required for maturation of excitability in flight promoting
647 dopaminergic neurons using genetic tools (Figure 4). We found that loss of *Trl* in the
648 fpDANs results in significant flight deficits, which could be partially rescued through
649 excess STIM (which raises SOCE). This indicates that increased Ca^{2+} entry through
650 Orai either activates residual Trl or alternate SOCE-responsive transcription factors to
651 induce *Set2* expression and rescue downstream gene expression essential for flight.

652 Although Trl function has been reported in the context of early embryonic
653 development, where it has been implicated in zygotic genome activation (Gaskill et al.,
654 2021) (ZGA), expression of *Hox* genes (Shimojima, 2003), dosage compensation
655 (Greenberg et al., 2004), and expression of a *Drosophila* voltage-gated calcium
656 channel subunit in germ cell development (Dorogova et al., 2014), this is the first ever
657 report of its role in regulating neuronal gene expression in the context of SOCE and
658 circuit maturation. The molecular mechanism by which Orai-mediated Ca^{2+} entry leads
659 to activation of Trl needs further elucidation. Our finding that CaMKII hyperactivation
660 partially rescues flight deficits caused by loss of Orai function, taken together with the
661 bioinformatic prediction for CaMKII-mediated Trl phosphorylation need to be
662 experimentally verified. Future studies could be directed towards looking at
663 interactions between these two proteins using in vitro biochemical assays.

664 In vitro studies on *Drosophila* Trl reveal that it utilizes a Q-rich intrinsically
665 disordered domain (IDD) to self-multimerize or interact with a wide range of accessory
666 proteins (Wilkins and Lis, 1999). Multimeric complexes of Trl reside on chromatin with
667 an exceptionally long residence time and maintain chromatin in an 'open' state (Tang
668 et al., 2022). Trl has also been reported to directly interact with components of the
669 Transcription initiation and elongation complex (Chopra et al., 2008; Li et al., 2013),

support long distance promoter-enhancer interactions (Mahmoudi, 2003), mediate active ATP-dependent chromatin remodeling by maintaining nucleosome free stretches (Tsukiyama et al., 1994), and regulating global gene expression by controlling transcriptional stalling and pausing (Tsai et al., 2016). A recent study demonstrates a role for Trl in chromatin folding in *Drosophila* neurons to enable cell type specific gene expression (Mohana et al., 2023). SOCE-dependent gene regulation may rely upon multiple transcription factors acting in concert in a cell type and developmental stage specific contexts, of which Trl may be just one. Future studies directed at other possible transcription factors downstream of SOCE would be of interest.

SOCE and the control of neuronal activity and cholinergic neuromodulation of a tripartite synapse in the mushroom body

Neurons undergo maturation of their electrical properties with a gradual increase in depolarizing responses and synaptic transmission over the course of pupal development (Jarvilehto and Finell, 1983). Here we show that a subset of dopaminergic neurons require a balance of ion channels for optimal excitation and inhibition essential for adult function. Neuromodulatory signals, such as acetylcholine are essential for acquiring this balance and act via an SOCE-Trl-Set2 mechanism during late pupal and early adult stages. The ability of *Set2* overexpression to rescue SOCE-deficient phenotypes (Figures 6A-C) indicates that anomalous gene expression is the underlying basis of this phenotype. Indeed, SOCE deficient dopaminergic neurons show reduced expression of an ensemble of voltage-gated ion channel genes (Figures 5E, F). including genes encoding the outward rectifying K^+ channel *shaw*, slow-inactivating voltage gated K^+ channel *shaker*, a Ca^{2+} gated K^+ channel *slowpoke* and *cacophony* a subunit of the voltage gated Ca^{2+} channel (Figure 6G). Ion channels like *Shaker* and *slowpoke* play an important role in establishing resting membrane potential (Singh and Wu, 1990), neuronal repolarisation (Lichtinghagen et al., 1990) and mediating afterhyperpolarisation (AHP) after repeated bouts of activity (Ping et al., 2011). Though dopaminergic neurons require *Set2* mediated expression of *cacophony* for excitability, *cacophony* is in itself insufficient to rescue the loss in excitability and flight deficits upon loss of SOCE (Figure 6J). Future experiments that

702 directly visualise electrophysiological responses of fpDANs from different genotypes
703 would help resolve the role of Cac and other ion channels and determine their
704 individual contributions to THD' neuronal activity and excitability. Both flight and KCl-
705 depolarisation in SOCE-deficient neurons could, however, be rescued by expression
706 of a heterologous depolarisation activated Na^+ channel NachBac (Nitabach, 2006)
707 (Figures 7B-D), which increases neuronal excitability by stimulating a low threshold
708 positive feedback loop and to a lesser extent by CsChrimson-mediated optogenetic
709 induction of neuronal activity (Figure 7E). The poorer rescue by optogenetic activation
710 may stem from the fact that sustained bursts of activity are non-physiological and can
711 deplete the readily releasable pool of neurotransmitters (Arrigoni and Saper, 2014;
712 Kaeser and Regehr, 2017). Other indirect forms of inducing neuronal hyperactivation
713 (Figures S7A, B) in SOCE-deficient neurons also achieved minor rescues in flight.
714 These results identify SOCE as a key driver downstream of developmentally salient
715 neuromodulatory signals for expression of an ion channels suite that enables
716 generation of intrinsic electrical properties and functional maturation of the PPL1
717 DANs, and the flight circuit.
718
719 **Limitations of this study**
720 Direct measurements of SOCE are generally performed in cultured cells by depletion
721 of ER-store Ca^{2+} in '0' Ca^{2+} medium, followed by Ca^{2+} -add back to measure SOCE.
722 In this study we were unable to perform similar SOCE measurements from the fpDANs
723 because they consist of 16-19 neurons in each hemisphere (PPL1 are 10-12 and
724 PPM3 are 6-7 cells; Pathak et al., 2015) and identifying these few neurons was not
725 technically feasible in culture. Measuring SOCE from these neurons *in vivo* was not
726 possible due to the presence of abundant extracellular Ca^{2+} in the brain. Due to these
727 reasons, we have relied upon using Carbachol to elicit IP_3-mediated Ca^{2+} release and
728 SOCE as a proxy for *in vivo* SOCE. In previous studies we have shown that Carbachol
729 treatment of cultured *Drosophila* neurons elicits IP_3-mediated Ca^{2+} release and SOCE
730 (Agrawal et al., 2010; Figure 8). Moreover, expression of $Orai^{E180A}$ completely blocks
731 SOCE as measured in primary cultures of dopaminergic neurons (Pathak et al., 2015;
732 Figure 1E) and CCh-induced IP_3-mediated Ca^{2+} release is tightly coupled to SOCE in
733 *Drosophila* neurons (Venkiteswaran and Hasan, 2009; Chakraborty et al., 2016;

734 Chakraborty et al., 2017). We posit that our measurements of CCh-evoked changes
735 in cellular Ca^{2+} reflect a composite of IP_3-mediated Ca^{2+} - release and SOCE.
736 Although we have provided compelling genetic evidence for Trl as an SOCE-
737 responsive transcription factor, the detailed biochemical basis of Trl activation was
738 beyond the scope of this study. We propose phosphorylation by CamKII as a possible
739 mechanism that needs further investigation.
740
741 **Methods**
742
743 **Fly maintenance**
744 *Drosophila* strains were grown on standard cornmeal medium consisting of 80 g corn
745 flour, 20 g glucose, 40 g sugar, 15 g yeast extract, 4 ml propionic acid, 5 ml p-
746 hydroxybenzoic acid methyl ester in ethanol and 5 ml ortho-butyric acid in a total
747 volume of 1 l (ND) at 25°C under a light-dark cycle of 12 h and 12 h. Canton S was
748 used as wild type throughout. Mixed sex populations were used for all experiments.
749 Several fly stocks used in this study were sourced using FlyBase (https://flybase.org),
750 which is supported by a grant from the National Human Genome Research Institute at
751 the US National Institutes of Health (#U41 HG000739), the British Medical Research
752 Council (#MR/N030117/1) and FlyBase users from across the world. The stocks were
753 obtained from the Bloomington Drosophila Stock Centre (BDSC) supported by NIH
754 P40OD018537. All fly stocks used and their sources are listed in Supplementary Table
755 1.
756
757 **Flight Assays**
758 Flight assays were performed as previously described (Manjila and Hasan, 2018).
759 Briefly, flies aged 3–5 days of either sex were tested in batches of 8–10 flies, and a
760 minimum of 30 flies were tested for each genotype. Adult flies were anaesthetized on
761 ice for 2–3 min and then tethered between at the head-thorax junction using a thin
762 metal wire and nail polish. Post recovery at room temperature for 2-3 min, an air puff
763 was provided as stimulus to initiate flight. Flight duration was recorded for each fly for
764 15 min. For all control genotypes, GAL4 or UAS strains were crossed to the Wild Type
765 strain, *Canton S*. Flight assays are represented in the form of a swarm plot, wherein
766 each dot represents a flight bout duration for a single fly. The colours indicate different

767 genotypes. The Δ Flight parameter refers to the mean difference for comparisons
768 against the shared CS control which is shown as a Cumming estimation plot(Ho et al.,
769 2018). On the lower axes, mean differences are plotted as bootstrap sampling
770 distributions. Each mean difference is depicted as a dot. Each 95% confidence interval
771 is indicated by the ends of the vertical error bars. Letters beneath each distribution
772 refer to statistically indistinguishable groups after performing a Kruskall-Wallis test
773 followed by a post hoc Mann-Whitney U-test ($p<0.05$).
774
775 **FACS**
776 Fluorescence-activated cell sorting (FACS) was used to enrich eGFP labelled DANs
777 from pupal/adult. The following genotypes were used for sorting: wild type
778 *(THD'GAL4> UAS-eGFP), Orai^{E180A} (THD'GAL4> Orai^{E180A})*, Set2^{IR-1} *(THD'GAL4>*
779 *Set2^{IR-1})*, *Orai^{E180A}; Set2^{OE} (THD'GAL4> Orai^{E180A}; Set2^{OE}), Set2^{OE} (THD'GAL4>*
780 *Set2^{OE}), Trl^{IR-1} (THD'GAL4> Trl^{IR-1})*. Approximately 100 pupae per sample were
781 washed in 1×PBS and 70% ethanol. Pupal/adult CNSs were dissected in Schneider's
782 medium (ThermoFisher Scientific) supplemented with 10% fetal bovine serum, 2%
783 PenStrep, 0.02 mM insulin, 20 mM glutamine and 0.04 mg/ml glutathione. Post
784 dissection, the CNSs were treated with an enzyme solution [0.75 g/l Collagenase and
785 0.4 g/l Dispase in Rinaldini's solution (8 mg/ml NaCl, 0.2 mg/ml KCl, 0.05 mg/ml
786 NaH2PO4, 1 mg/ml NaHCO3 and 0.1 mg/ml glucose)] at room temperature for 30 min.
787 They were then washed and resuspended in ice-cold Schneider's medium and gently
788 triturated several times using a pipette tip to obtain a single-cell suspension. This
789 suspension was then passed through a 40 mm mesh filter to remove clumps and kept
790 on ice until sorting (less than 1 h). Flow cytometry was performed on a FACS Aria
791 Fusion cell sorter (BD Biosciences) with a 100 mm nozzle at 60 psi. The threshold for
792 GFP-positive cells was set using dissociated neurons from a non GFP-expressing
793 wild-type strain (*Canton S*). The same gating parameters were used to sort other
794 genotypes in the experiment. GFP-positive cells were collected directly in TRIzol and
795 then frozen immediately in dry ice until further processing. Details for all reagents used
796 are listed in Supplementary Table 2.
797
798 **RNA-Seq**

799 RNA from at least 600 sorted *THD'* DANs from the relevant genotypes, expressing
800 *UAS-eGFP* was subjected to 14 cycles of PCR amplification (SMARTer Seq V4 Ultra
801 Low Input RNA Kit; Takara Bio). 1 ng of amplified RNA was used to prepare cDNA
802 libraries (Nextera XT DNA library preparation kit; Illumina). cDNA libraries for 4
803 biological replicates for both control (*THD'GAL4/+*) and experimental
804 (*THD'GAL4>UAS-Orai*^{E180A}) genotypes were run on a Hiseq2500 platform. 50-70
805 million unpaired sequencing reads per sample were aligned to the dm6 release of the
806 *Drosophila* genome using HISAT2(Kim et al., 2015, 2019) and an overall alignment
807 rate of 95.2-96.8% was obtained for all samples. Featurecounts(Liao et al., 2014) was
808 used to assign the mapped sequence reads to the genome and obtain read counts.
809 Differential expression analysis was performed using three independent methods:
810 DESeq2(Love et al., 2014), limma-voom(Ritchie et al., 2015), and edgeR(Robinson et
811 al., 2009). A fold change cutoff of a minimum twofold change was used. Significance
812 cutoff was set at an FDR-corrected P value of 0.05 for DESeq2 and edgeR.
813 Volcanoplots were generated using VolcaNoseR (https://huygens.science.uva.nl/).
814 Comparison of gene lists and generation of Venn diagrams was performed using
815 Whitehead BaRC public tools (http://jura.wi.mit.edu/bioc/tools/). Gene ontology
816 analysis for molecular function was performed using DAVID(Huang et al., 2008, 2009).
817 Developmental gene expression levels were measured for downregulated genes
818 using FlyBase(Larkin et al., 2020) and DGET(Hu et al., 2017)
819 (www.flyrnai.org/tools/dget/web/), and were plotted as a heatmap using ClustVis
820 (Metsalu and Vilo, 2015) (https://biit.cs.ut.ee/clustvis/).
821

822 **qRT-PCRs**

823 Central nervous systems (CNSs) of the appropriate genotype and age were dissected
824 in 1× phosphate-buffered saline (PBS; 137 mM NaCl, 2.7 mM KCl, 10 mM Na_2HPO_4
825 and 1.8 mM KH_2PO_4) prepared in double distilled water treated with DEPC. Each
826 sample consisted of five CNS homogenized in 500 µl of TRIzol (Ambion,
827 ThermoFisher Scientific) per sample. At least three biological replicate samples were
828 made for each genotype. After homogenization the sample was kept on ice and either
829 processed further within 30 min or stored at −80°C for up to 4 weeks before
830 processing. RNA was isolated following the manufacturer's protocol. Purity of the
831 isolated RNA was estimated by NanoDrop spectrophotometer (ThermoFisher

832 Scientific) and integrity was checked by running it on a 1% Tris-EDTA agarose gel.
833 Approximately 100 ng of total RNA was used per sample for cDNA synthesis. DNAse
834 treatment and first-strand synthesis were performed as described previously(Pathak
835 et al., 2015). Quantitative real time PCRs (qPCRs) were performed in a total volume
836 of 10 µl with Kapa SYBR Fast qPCR kit (KAPA Biosystems) on an ABI 7500 fast
837 machine operated with ABI 7500 software (Applied Biosystems). Technical duplicates
838 were performed for each qPCR reaction. The fold change of gene expression in any
839 experimental condition relative to wild type was calculated as $2^{-\Delta\Delta Ct}$, where $\Delta\Delta C_t$=[C_t
840 (target gene) –C_t (rp49)] Expt. – [C_t (target gene) – C_t (rp49)]. Primers specific for rp49
841 and ac5c were used as internal controls. Sequences of all primers used are provided
842 in Supplementary Table 3.
843
844 **Functional imaging**
845 Adult brains were dissected in adult hemolymph-like saline (AHL: 108 mM NaCl, 5 mM
846 KCl, 2 mM CaCl2, 8.2 mM $MgCl_2$, 4 mM $NaHCO_3$, 1 mM NaH_2PO_4, 5 mM Trehalose,
847 10 mM Sucrose, 5 mM Tris, pH 7.5) after embedded in a drop of 0.1% low-melting
848 agarose (Invitrogen). Embedded brains were bathed in AHL and then subjected to
849 functional imaging. The genetically encoded calcium sensor *GCaMP6m* (Chen et al.,
850 2013) was used to record changes in intracellular cytosolic Ca^{2+} in response to
851 stimulation with carbachol or KCl. The GRAB-DA sensor (Sun et al., 2018) was used
852 to measure evoked dopamine release. Images were taken as a time series on a xy
853 plane at an interval of 1 s using a 20× objective with an NA of 0.7 on an Olympus
854 FV3000 inverted confocal microscope. A 488 nm laser line was used to record
855 GCaMP6m / GRAB-DA measurements. All live-imaging experiments were performed
856 with at least 10 independent brain preparations. For measuring evoked responses,
857 KCl/Carbachol, was added on top of the samples. For optogenetics experiments, flies
858 were reared on medium supplemented with 200 µM ATR (all trans retinal), following
859 which neuronal activation was achieved using a 633-nm laser line to stimulate
860 *CsChrimson* (Klapoetke et al., 2014) while simultaneously acquiring images with the
861 488 nm laser line, and the images were acquired every 1 s. The raw images were
862 extracted using FIJI (Schindelin et al., 2012) (based on ImageJ version 2.1.0/1.53c).
863 ΔF/F was calculated from selected regions of interest (ROIs) using the formula
864 ΔF/F=(Ft-F0)/F0, where Ft is the fluorescence at time t and F0 is baseline

865 fluorescence corresponding to the average fluorescence over the first 40-time frames.
866 Mean ΔF/F time-lapses were plotted using PlotTwist (Goedhart, 2020)
867 (https://huygens.science.uva.nl/PlotTwist/). A shaded error bar around the mean
868 indicates the 95% confidence interval for CCh (50 μM) or KCl (70 mM) responses.
869 Peaks for individual cellular responses for each genotype was calculated from before
870 or after the point of stimulation, using Microsoft Excel and plotted as a paired plot using
871 SuperPlotsOfData (Goedhart, 2021)
872 (https://huygens.science.uva.nl/SuperPlotsOfData/). Boxplots were plotted using
873 PlotsOfData (Postma and Goedhart, 2019)
874 (https://huygens.science.uva.nl/PlotsOfData/).
875
876 **Immunohistochemistry**
877 Immunostaining of larval *Drosophila* brains was performed as described
878 previously(Daniels et al., 2008). Briefly, adult brains were dissected in 1x phosphate
879 buffered saline (PBS) and fixed with 4% Paraformaldehyde. The dissected brains were
880 washed 3-4 times with 0.2% phosphate buffer, pH 7.2 containing 0.2% Triton-X 100
881 (PTX) and blocked with 0.2% PTX containing 5% normal goat serum (NGS) for 2 hours
882 at room temperature. Respective primary antibodies were incubated overnight (14–16
883 hr) at 4°C. After washing 3-4 times with 0.2% PTX at room temperature, they were
884 incubated in the respective secondary antibodies for 2 hr at room temperature. The
885 following primary antibodies were used: chick anti-GFP antibody (1:10,000; A6455,
886 Life Technologies), mouse anti-nc82 (anti-brp) antibody (1:50), rabbit anti-H3K36me3,
887 mouse anti-RFP. Secondary antibodies were used at a dilution of 1:400 as follows:
888 anti-rabbit Alexa Fluor 488 (#A11008, Life Technologies), anti-mouse Alexa Fluor 488
889 (#A11001, Life Technologies). Confocal images were obtained on the Olympus
890 Confocal FV1000 microscope (Olympus) with a 40x, 1.3 NA objective or with a 60x,
891 1.4 NA objective. Imaging for axonal arbors within the mushroom body γ lobe was
892 performed on the Zeiss LSM980 system with AiryScan 2. Images were visualized
893 using either the FV10-ASW 4.0 viewer (Olympus) or Fiji (Schindelin et al., 2012).
894 Details for all reagents used are listed in Supplementary Table 2.
895
896 **Western Blotting**

897 Adult CNSs of appropriate genotypes were dissected in ice-cold PBS. Between 5 and
898 10 brains were homogenized in 50 µl of NETN buffer [100 mM NaCl, 20 mM Tris-Cl
899 (pH 8.0), 0.5 mM EDTA, 0.5% Triton-X-100, 1× Protease inhibitor cocktail (Roche)].
900 The homogenate (10-15 µl) was run on an 8% SDS-polyacrylamide gel. The protein
901 was transferred to a PVDF membrane by standard semi-dry transfer protocols (10 V
902 for 10 min). The membrane was incubated in the primary antibody overnight at 4°C.
903 Primary antibodies were used at the following dilutions: rabbit anti-H3K36me3
904 (1:5000, Abcam, ab9050) and rabbit anti-H3 (1:5000, Abcam, ab12079). Secondary
905 antibodies conjugated with horseradish peroxidase were used at dilution of 1:3000
906 (anti-rabbit HRP; 32260, Thermo Scientific). Protein was detected by a
907 chemiluminescent reaction (WesternBright ECL, Advansta K12045-20). Blots were
908 first probed for H3K36me3, stripped with a solution of 3% glacial acetic acid for 10
909 min, followed by re-probing with the anti-H3 antibody.
910
911 **In silico ChIP-Seq Analysis**
912 H3K36me3 enrichment data was obtained from a ChIP-chip dataset (ID_301)
913 generated in *Drosophila* ML-DmBG3-c2 cells submitted to modEncode(Celniker et al.,
914 2009; modENCODE Consortium et al., 2010). Enrichment scores for genomic regions
915 were calculated using 'computematrix' and plotted as a tag density plot using
916 'plotHeatmap' from deeptools2(Ramírez et al., 2016). All genes were scaled to 2 kb
917 with a flanking region of 250 bp on either end. A 50 bp length of non-overlapping bins
918 was used for averaging the score over each region length. Genes were sorted based
919 on mean enrichment scores and displayed on the heatmap in descending order.
920
921 **Statistical tests**
922 Non-parametric tests were employed to test significance for data that did not follow a
923 normal distribution. Significant differences between experimental genotypes and
924 relevant controls were tested either with the Kruskal-Wallis test followed by Dunn's
925 multiple comparison test (for multiple comparisons) or with Mann-Whitney U tests (for
926 pairwise comparisons). Data with normal distribution were tested by the Student's T-
927 test. Statistical tests and p-values are mentioned in each figure legend. For calculation
928 and representation of effect size, estimationstats.com was used.

929 **Acknowledgements**

930 We acknowledge the Central Imaging and Flow Cytometry Facility (CIFF, NCBS) for
931 maintenance of microscopes and the *Drosophila* facility (Flyfacility, NCBS) for Fly
932 stock maintenance and development of transgenics. We thank Nandashree KS for
933 helping with super resolution imaging on the Zeiss 980 Airyscan system.

934

935 **Competing Interests**

936 The authors declare no competing interests

937

938 **Funding**

939 This work was funded by grant No. BT/PR28450/MED/122/166/2018 from the
940 Department of Biotechnology, Govt. of India and core support by NCBS, TIFR. RM
941 and SR received graduate student fellowships from NCBS, TIFR.

942

943 **Data availability**

944 The RNA Sequencing data has been submitted to GEO under accession number
945 GSE230134.

946

947 **References**

948 Agrawal N, Venkiteswaran G, Sadaf S, Padmanabhan N, Banerjee S, Hasan G.
949 (2010). Inositol 1,4,5-Trisphosphate Receptor and dSTIM Function in Drosophila
950 Insulin-Producing Neurons Regulates Systemic Intracellular Calcium
951 Homeostasis and Flight. *J Neurosci.*, 30, 1301-1313.
952 http://doi.org/10.1523/jneurosci.3668-09.2010
953 Agrawal, T., Sadaf, S., & Hasan, G. (2013). A Genetic RNAi Screen for IP3/Ca2+
954 Coupled GPCRs in Drosophila Identifies the PdfR as a Regulator of Insect

Flight. *PLoS Genetics*, *9*, e1003849. https://doi.org/10.1371/journal.pgen.1003849

Akin, O., & Zipursky, S. L. (2020). Activity regulates brain development in the fly. *Current Opinion in Genetics & Development*, *65*, 8–13. https://doi.org/10.1016/j.gde.2020.04.005

Ardehali, M. B., Mei, A., Zobeck, K. L., Caron, M., Lis, J. T., & Kusch, T. (2011). *Drosophila*Set1 is the major histone H3 lysine 4 trimethyltransferase with role in transcription. *The EMBO Journal*, *30*, 2817–2828. https://doi.org/10.1038/emboj.2011.194

Arrigoni, E., & Saper, C. B. (2014). What optogenetic stimulation is telling us (and failing to tell us) about fast neurotransmitters and neuromodulators in brain circuits for wake–sleep regulation. *Current Opinion in Neurobiology*, *29*, 165–171. https://doi.org/10.1016/j.conb.2014.07.016

Aso, Y., Hattori, D., Yu, Y., Johnston, R. M., Iyer, N. A., Ngo, T.-T. B., Dionne, H., Abbott, L. F., Axel, R., Tanimoto, H., & Rubin, G. M. (2014). The neuronal architecture of the mushroom body provides a logic for associative learning. *ELife*, *3*, e04577. https://doi.org/10.7554/eLife.04577

Aso, Y., & Rubin, G. M. (2016). Dopaminergic neurons write and update memories with cell-type-specific rules. *ELife*, *5*. https://doi.org/10.7554/eLife.16135

Bannister, A. J., & Kouzarides, T. (2011). Regulation of Chromatin by Histone Modifications. *Cell Research*, *21*, 381–395. https://doi.org/10.1038/cr.2011.22

Berry, J. A., Cervantes-Sandoval, I., Chakraborty, M., & Davis, R. L. (2015). Sleep Facilitates Memory by Blocking Dopamine Neuron-Mediated Forgetting. *Cell*, *161*, 1656–1667. https://doi.org/10.1016/j.cell.2015.05.027

Brimblecombe, K. R., Gracie, C. J., Platt, N. J., & Cragg, S. J. (2015). Gating of dopamine transmission by calcium and axonal N-, Q-, T- and L-type voltage-gated calcium channels differs between striatal domains. *The Journal of Physiology*, *593*, 929–946. https://doi.org/10.1113/jphysiol.2014.285890

Cai, Y., Zhang, Y., Loh, Y. P., Tng, J. Q., Lim, M. C., Cao, Z., Raju, A., Lieberman Aiden, E., Li, S., Manikandan, L., Tergaonkar, V., Tucker-Kellogg, G., & Fullwood, M. J. (2021). H3K27me3-rich genomic regions can function as silencers to repress gene expression via chromatin interactions. *Nature*

Communications, *12*. https://doi.org/10.1038/s41467-021-20940-y

Celniker, S. E., Dillon, L. A. L., Gerstein, M. B., Gunsalus, K. C., Henikoff, S., Karpen, G. H., Kellis, M., Lai, E. C., Lieb, J. D., MacAlpine, D. M., Micklem, G., Piano, F., Snyder, M., Stein, L., White, K. P., & Waterston, R. H. (2009). Unlocking the secrets of the genome. *Nature*, *459*(7249), 927–930. https://doi.org/10.1038/459927a

Cervantes-Sandoval, I., Phan, A., Chakraborty, M., & Davis, R. L. (2017). Reciprocal synapses between mushroom body and dopamine neurons form a positive feedback loop required for learning. *ELife*, *6*. https://doi.org/10.7554/elife.23789

Chakraborty S, Deb BK, Chorna T, Konieczny V, Taylor CW, Hasan G. (2016). Mutant IP3 receptors attenuate store-operated Ca2+ entry by destabilizing STIM-Orai interactions in *Drosophila* neurons. *J Cell Sci.*, 129, 3903-3910. http://doi.org/10.1242/jcs.191585

Chakraborty S, Hasan G. (2017). Spontaneous Ca^{2+} Influx in *Drosophila* Pupal Neurons Is Modulated by IP_3-Receptor Function and Influences Maturation of the Flight Circuit. Front Mol Neurosci., 20, 10:111. http://doi.org/10.3389/fnmol.2017.00111.

Chen, T.-W., Wardill, T. J., Sun, Y., Pulver, S. R., Renninger, S. L., Baohan, A., Schreiter, E. R., Kerr, R. A., Orger, M. B., Jayaraman, V., Looger, L. L., Svoboda, K., & Kim, D. S. (2013). Ultrasensitive fluorescent proteins for imaging neuronal activity. *Nature*, *499*, 295–300. https://doi.org/10.1038/nature12354

Chopra, V. S., Srinivasan, A., Kumar, R. P., Mishra, K., Basquin, D., Docquier, M., Seum, C., Pauli, D., & Mishra, R. K. (2008). Transcriptional activation by GAGA factor is through its direct interaction with dmTAF3. *Developmental Biology*, *317*, 660–670. https://doi.org/10.1016/j.ydbio.2008.02.008

Ciceri, G., Cho, H., Kshirsagar, M., Baggiolini, A., Aromolaran, K. A., Walsh, R. M., Goldstein, P. A., Koche, R. P., Leslie, C. S., & Studer, L. (2022). An epigenetic barrier sets the timing of human neuronal maturation. *BioArxiv*. https://doi.org/10.1101/2022.06.02.490114

Daniels, R. W., Gelfand, M. V, Collins, C. A., & DiAntonio, A. (2008). Visualizing glutamatergic cell bodies and synapses inDrosophila larval and adult CNS. *The Journal of Comparative Neurology*, *508*, 131–152.

1019 https://doi.org/10.1002/cne.21670
1020 Deb BK, Pathak T, Hasan G. (2016). Store-independent modulation of Ca2+ entry
1021 through Orai by Septin 7. *Nat Commun*. 2016. 7,11751.
1022 http://doi.org/10.1038/ncomms11751
1023 Depetris-Chauvin A, Berni J, Aranovich EJ, Muraro NI, Beckwith EJ, Ceriani MF.
1024 Adult-specific electrical silencing of pacemaker neurons uncouples molecular
1025 clock from circadian outputs. Curr Biol. 2011. 21:1783-1793. doi:
1026 10.1016/j.cub.2011.09.027.
1027 Dillon, S. C., Zhang, X., Trievel, R. C., & Cheng, X. (2005). The SET-domain protein
1028 superfamily: protein lysine methyltransferases. *Genome Biology*, *6*, 227.
1029 https://doi.org/10.1186/gb-2005-6-8-227
1030 Dorogova, N. V, Fedorova, E. V, Bolobolova, E. U., Ogienko, A. A., & Baricheva, E.
1031 M. (2014). GAGA protein is essential for male germ cell development
1032 inDrosophila. *Genesis*, *52*, 738–751. https://doi.org/10.1002/dvg.22789
1033 Ebihara, T., Guo, F., Zhang, L., Kim, J. Y., & Saffen, D. (2006). Muscarinic
1034 Acetylcholine Receptors Stimulate Ca2+ Influx in PC12D Cells Predominantly
1035 via Activation of Ca2+ Store–Operated Channels. *The Journal of Biochemistry*,
1036 *139*, 449–458. https://doi.org/10.1093/jb/mvj064
1037 Finogenova, K., Bonnet, J., Poepsel, S., Schäfer, I. B., Finkl, K., Schmid, K., Litz, C.,
1038 Strauss, M., Benda, C., & Müller, J. (2020). Structural basis for PRC2 decoding
1039 of active histone methylation marks H3K36me2/3. *ELife*, *9*.
1040 https://doi.org/10.7554/elife.61964
1041 Gaskill, M. M., Gibson, T. J., Larson, E. D., & Harrison, M. M. (2021). GAF is
1042 essential for zygotic genome activation and chromatin accessibility in the early
1043 Drosophila embryo. *ELife*, *10*. https://doi.org/10.7554/elife.66668
1044 Geng, H., Chen, H., Wang, H., & Wang, L. (2021). The Histone Modifications of
1045 Neuronal Plasticity. *Neural Plasticity*, *2021*, 1–7.
1046 https://doi.org/10.1155/2021/6690523
1047 Gilbert, L. A., Larson, M. H., Morsut, L., Liu, Z., Brar, G. A., Torres, S. E., Stern-
1048 Ginossar, N., Brandman, O., Whitehead, E. H., Doudna, J. A., Lim, W. A.,
1049 Weissman, J. S., & Qi, L. S. (2013). CRISPR-Mediated Modular RNA-Guided
1050 Regulation of Transcription in Eukaryotes. *Cell*, *154*, 442–451.

https://doi.org/10.1016/j.cell.2013.06.044

Goedhart, J. (2020). PlotTwist: A web app for plotting and annotating continuous data. *PLOS Biology*, *18*, e3000581. https://doi.org/10.1371/journal.pbio.3000581

Goedhart, J. (2021). SuperPlotsOfData—a web app for the transparent display and quantitative comparison of continuous data from different conditions. *Molecular Biology of the Cell*, *32*, 470–474. https://doi.org/10.1091/mbc.e20-09-0583

Govorunova, E. G., Sineshchekov, O. A., Janz, R., Liu, X., & Spudich, J. L. (2015). Natural light-gated anion channels: A family of microbial rhodopsins for advanced optogenetics. *Science*, *349*, 647–650. https://doi.org/10.1126/science.aaa7484

Greenberg, A. J., Yanowitz, J. L., & Schedl, P. (2004). The Drosophila GAGA Factor Is Required for Dosage Compensation in Males and for the Formation of the Male-Specific-Lethal Complex Chromatin Entry Site at 12DE. *Genetics*, *166*, 279–289. https://doi.org/10.1534/genetics.166.1.279

Gu, X., & Spitzer, N. C. (1995). Distinct aspects of neuronal differentiation encoded by frequency of spontaneous Ca2+ transients. *Nature*, *375*, 784–787. https://doi.org/10.1038/375784a0

Hardie, R. C., Peretz, A., Suss-Toby, E., Rom-Glas, A., Bishop, S. A., Selinger, Z., & Minke, B. (1993). Protein kinase C is required for light adaptation in Drosophila photoreceptors. *Nature*, *363*, 634–637. https://doi.org/10.1038/363634a0

Hasan, G., & Sharma, A. (2020). Regulation of neuronal physiology by Ca2+ release through the IP3R. *Current Opinion in Physiology*, *17*, 1–8. https://doi.org/10.1016/j.cophys.2020.06.001

Ho, J., Tumkaya, T., Aryal, S., Choi, H., & Claridge-Chang, A. (2018). Moving beyond *P* values: Everyday data analysis with estimation plots. *BioArxiv*. https://doi.org/10.1101/377978

Hogan, P. G., Chen, L., Nardone, J., & Rao, A. (2003). Transcriptional regulation by calcium, calcineurin, and NFAT. *Genes & Development*, *17*, 2205–2232. https://doi.org/10.1101/gad.1102703

Hu, Y., Comjean, A., Perrimon, N., & Mohr, S. E. (2017). The Drosophila Gene Expression Tool (DGET) for expression analyses. *BMC Bioinformatics*, *18*(1), 1–9. https://doi.org/10.1186/s12859-017-1509-z

1083 Huang, D. W., Sherman, B. T., & Lempicki, R. A. (2008). Systematic and integrative
1084 analysis of large gene lists using DAVID bioinformatics resources. *Nature*
1085 *Protocols*, *4*, 44–57. https://doi.org/10.1038/nprot.2008.211
1086 Huang, D. W., Sherman, B. T., & Lempicki, R. A. (2009). Systematic and integrative
1087 analysis of large gene lists using DAVID bioinformatics resources. *Nature*
1088 *Protocols*, *4*(1), 44–57. https://doi.org/10.1038/nprot.2008.211
1089 Jarvilehto, M., & Finell, N. (1983). Development of the function of visual receptor
1090 cells during the pupal life of the flyCalliphora. *Journal of Comparative*
1091 *Physiology ? A*, *150*, 529–536. https://doi.org/10.1007/bf00609579
1092 Johns, D. C., Marx, R., Mains, R. E., O'Rourke, B., & Marbán, E. (1999). Inducible
1093 Genetic Suppression of Neuronal Excitability. *The Journal of Neuroscience*, *19*,
1094 1691–1697. https://doi.org/10.1523/jneurosci.19-05-01691.1999
1095 Johnson-Venkatesh, E. M., Khan, M. N., Murphy, G. G., Sutton, M. A., & Umemori,
1096 H. (2015). Excitability governs neural development in a hippocampal region
1097 specific manner. *Development*. https://doi.org/10.1242/dev.121202
1098 Joshi, R., Venkatesh, K., Srinivas, R., Nair, S., & Hasan, G. (2004). Genetic
1099 Dissection of itpr Gene Function Reveals a Vital Requirement in Aminergic Cells
1100 of Drosophila Larvae. *Genetics*, *166*(1), 225–236.
1101 https://doi.org/10.1534/genetics.166.1.225
1102 Kadas D, Tzortzopoulos A, Skoulakis EM, Consoulas C. (2012). Constitutive
1103 activation of Ca2+/calmodulin-dependent protein kinase II during development
1104 impairs central cholinergic transmission in a circuit underlying escape behavior
1105 in Drosophila. J Neurosci.,32, 170-82.
1106 doi: 10.1523/JNEUROSCI.6583-10.2012.
1107 Kaeser, P. S., & Regehr, W. G. (2017). The readily releasable pool of synaptic
1108 vesicles. *Current Opinion in Neurobiology*, *43*, 63–70.
1109 https://doi.org/10.1016/j.conb.2016.12.012
1110 Keyser, P., Borge-Renberg, K., & Hultmark, D. (2007). The Drosophila NFAT
1111 homolog is involved in salt stress tolerance. *Insect Biochemistry and Molecular*
1112 *Biology*, *37*, 356–362. https://doi.org/10.1016/j.ibmb.2006.12.009
1113 Kim, D., Langmead, B., & Salzberg, S. L. (2015). HISAT: A fast spliced aligner with
1114 low memory requirements. *Nature Methods*, *12*(4), 357–360.

https://doi.org/10.1038/nmeth.3317

Kim, D., Paggi, J. M., Park, C., Bennett, C., & Salzberg, S. L. (2019). Graph-based genome alignment and genotyping with HISAT2 and HISAT-genotype. *Nature Biotechnology*, *37*(8), 907–915. https://doi.org/10.1038/s41587-019-0201-4

Kishi, Y., & Gotoh, Y. (2018). Regulation of Chromatin Structure During Neural Development. *Frontiers in Neuroscience*, *12*. https://doi.org/10.3389/fnins.2018.00874

Kitamoto, T. (2001). Conditional modification of behavior inDrosophila by targeted expression of a temperature-sensitiveshibire allele in defined neurons. *Journal of Neurobiology*, *47*, 81–92. https://doi.org/10.1002/neu.1018

Klapoetke, N. C., Murata, Y., Kim, S. S., Pulver, S. R., Birdsey-Benson, A., Cho, Y. K., Morimoto, T. K., Chuong, A. S., Carpenter, E. J., Tian, Z., Wang, J., Xie, Y., Yan, Z., Zhang, Y., Chow, B. Y., Surek, B., Melkonian, M., Jayaraman, V., Constantine-Paton, M., … Boyden, E. S. (2014). Independent optical excitation of distinct neural populations. *Nature Methods*, *11*, 338–346. https://doi.org/10.1038/nmeth.2836

Kong, E. C., Woo, K., Li, H., Lebestky, T., Mayer, N., Sniffen, M. R., Heberlein, U., Bainton, R. J., Hirsh, J., & Wolf, F. W. (2010). A Pair of Dopamine Neurons Target the D1-Like Dopamine Receptor DopR in the Central Complex to Promote Ethanol-Stimulated Locomotion in Drosophila. *PLoS ONE*, *5*. https://doi.org/10.1371/journal.pone.0009954

Krogan, N. J., Kim, M., Tong, A., Golshani, A., Cagney, G., Canadien, V., Richards, D. P., Beattie, B. K., Emili, A., Boone, C., Shilatifard, A., Buratowski, S., & Greenblatt, J. (2003). Methylation of Histone H3 by Set2 in *Saccharomyces cerevisiae* Is Linked to Transcriptional Elongation by RNA Polymerase II. *Molecular and Cellular Biology*, *23*, 4207–4218. https://doi.org/10.1128/mcb.23.12.4207-4218.2003

Larkin, A., Marygold, S. J., Antonazzo, G., Attrill, H., dos Santos, G., Garapati, P. V, Goodman, J. L., Gramates, L. S., Millburn, G., Strelets, V. B., Tabone, C. J., Thurmond, J., Perrimon, N., Gelbart, S. R., Agapite, J., Broll, K., Crosby, M., dos Santos, G., Falls, K., … Lovato, T. (2020). FlyBase: updates to the Drosophila melanogaster knowledge base. *Nucleic Acids Research*, *49*, D899–D907.

https://doi.org/10.1093/nar/gkaa1026

Leinwand, S. G., & Scott, K. (2021). Juvenile hormone drives the maturation of spontaneous mushroom body neural activity and learned behavior. *Neuron*, *109*, 1836-1847.e5. https://doi.org/10.1016/j.neuron.2021.04.006

Levine, R. B. (1984). Changes in Neuronal Circuits During Insect Metamorphosis. *Journal of Experimental Biology*, *112*, 27–44. https://doi.org/10.1242/jeb.112.1.27

Li, J., Liu, Y., Rhee, H. S., Ghosh, S. K. B., Bai, L., Pugh, B. F., & Gilmour, D. S. (2013). Kinetic Competition between Elongation Rate and Binding of NELF Controls Promoter-Proximal Pausing. *Molecular Cell*, *50*(5), 711–722. https://doi.org/10.1016/j.molcel.2013.05.016

Liao, Y., Smyth, G. K., & Shi, W. (2014). FeatureCounts: An efficient general purpose program for assigning sequence reads to genomic features. *Bioinformatics*, *30*(7), 923–930. https://doi.org/10.1093/bioinformatics/btt656

Lichtinghagen, R., Stocker, M., Wittka, R., Boheim, G., Stühmer, W., Ferrus, A., & Pongs, O. (1990). Molecular basis of altered excitability in Shaker mutants of Drosophila melanogaster. *The EMBO Journal*, *9*, 4399–4407. https://doi.org/10.1002/j.1460-2075.1990.tb07890.x

Lieberman, O. J., McGuirt, A. F., Mosharov, E. V, Pigulevskiy, I., Hobson, B. D., Choi, S., Frier, M. D., Santini, E., Borgkvist, A., & Sulzer, D. (2018). Dopamine Triggers the Maturation of Striatal Spiny Projection Neuron Excitability during a Critical Period. *Neuron*, *99*, 540-554.e4. https://doi.org/10.1016/j.neuron.2018.06.044

Liu, C., Plaçais, P.-Y., Yamagata, N., Pfeiffer, B. D., Aso, Y., Friedrich, A. B., Siwanowicz, I., Rubin, G. M., Preat, T., & Tanimoto, H. (2012). A subset of dopamine neurons signals reward for odour memory in Drosophila. *Nature*, *488*, 512–516. https://doi.org/10.1038/nature11304

Lomaev, D., Mikhailova, A., Erokhin, M., Shaposhnikov, A. V, Moresco, J. J., Blokhina, T., Wolle, D., Aoki, T., Ryabykh, V., Yates, J. R., Shidlovskii, Y. V, Georgiev, P., Schedl, P., & Chetverina, D. (2017). The GAGA factor regulatory network: Identification of GAGA factor associated proteins. *PLOS ONE*, *12*, e0173602. https://doi.org/10.1371/journal.pone.0173602

1179 Love, M. I., Huber, W., & Anders, S. (2014). Moderated estimation of fold change
1180 and dispersion for RNA-seq data with DESeq2. *Genome Biology*, *15*(12), 1–21.
1181 https://doi.org/10.1186/s13059-014-0550-8
1182 Mahmoudi, T. (2003). GAGA facilitates binding of Pleiohomeotic to a chromatinized
1183 Polycomb response element. *Nucleic Acids Research*, *31*(14), 4147–4156.
1184 https://doi.org/10.1093/nar/gkg479
1185 Malik B, Hodge J. 2014. CASK and CaMKII function in Drosophila memory. Front
1186 Neurosci., 8:178.
1187 doi: 10.3389/fnins.2014.00178
1188 Manjila, S., & Hasan, G. (2018). Flight and Climbing Assay for Assessing Motor
1189 Functions in Drosophila. *BIO-PROTOCOL*, *8*.
1190 https://doi.org/10.21769/bioprotoc.2742
1191 Mao, Z., & Davis, R. (2009). Eight different types of dopaminergic neurons innervate
1192 the Drosophila mushroom body neuropil: anatomical and physiological
1193 heterogeneity. *Frontiers in Neural Circuits*, *3*.
1194 https://doi.org/10.3389/neuro.04.005.2009
1195 Marder, E. (2012). Neuromodulation of Neuronal Circuits: Back to the Future.
1196 *Neuron*, *76*, 1–11. https://doi.org/10.1016/j.neuron.2012.09.010
1197 Margueron, R., & Reinberg, D. (2011). The Polycomb complex PRC2 and its mark in
1198 life. *Nature*, *469*, 343–349. https://doi.org/10.1038/nature09784
1199 Mayseless, O., Shapira, G., Rachad, E. Y., Fiala, A., & Schuldiner, O. (2023).
1200 Neuronal excitability as a regulator of circuit remodeling. *Current Biology*, *33*,
1201 981-989.e3. https://doi.org/10.1016/j.cub.2023.01.032
1202 McGuire, S. E., Mao, Z., & Davis, R. L. (2004). Spatiotemporal Gene Expression
1203 Targeting with the TARGET and Gene-Switch Systems in Drosophila. *Science*
1204 *Signaling*, *2004*, pl6–pl6. https://doi.org/10.1126/stke.2202004pl6
1205 McKinney, A., Petrova, R., & Panagiotakos, G. (2022). Calcium and activity-
1206 dependent signaling in the developing cerebral cortex. *Development*, *149*.
1207 https://doi.org/10.1242/dev.198853
1208 Megha, & Hasan, G. (2017). IP3R-mediated Ca2+ release regulates protein
1209 metabolism in drosophila neuroendocrine cells: Implications for development
1210 under nutrient stress. *Development (Cambridge)*, *144*(8), 1484–1489.

https://doi.org/10.1242/dev.145235

Mehren JE, Griffith LC. (2004). Calcium-independent calcium/calmodulin-dependent protein kinase II in the adult Drosophila CNS enhances the training of pheromonal cues. J Neurosci., 24,10584-93. doi: 10.1523/JNEUROSCI.3560-04.2004

Metsalu, T., & Vilo, J. (2015). ClustVis: A web tool for visualizing clustering of multivariate data using Principal Component Analysis and heatmap. *Nucleic Acids Research*, *43*(W1), W566–W570. https://doi.org/10.1093/nar/gkv468

Mitra, R., & Hasan, G. (2022). Store-operated Ca2+ entry regulates neuronal gene expression and function. *Current Opinion in Neurobiology*, *73*, 102520. https://doi.org/10.1016/j.conb.2022.01.005

Mitra, R., Richhariya, S., Jayakumar, S., Notani, D., & Hasan, G. (2020). IP3/Ca2+ signals regulate larval to pupal transition under nutrient stress through the H3K36 methyltransferase dSET2. *BioRxiv*. https://doi.org/10.1101/2020.11.25.399329

modENCODE Consortium, Roy, S., Ernst, J., Kharchenko, P. V, Kheradpour, P., Negre, N., Eaton, M. L., Landolin, J. M., Bristow, C. A., Ma, L., Lin, M. F., Washietl, S., Arshinoff, B. I., Ay, F., Meyer, P. E., Robine, N., Washington, N. L., Di Stefano, L., Berezikov, E., … Kellis, M. (2010). Identification of functional elements and regulatory circuits by Drosophila modENCODE. *Science (New York, N.Y.)*, *330*, 1787–1797. https://doi.org/10.1126/science.1198374

Mohana G, Dorier J, Li X, Mouginot M, Smith RC, Malek H, Leleu M, Rodriguez D, Khadka J, Rosa P, Cousin P, Iseli C, Restrepo S, Guex N, McCabe BD, Jankowski A, Levine MS, Gambetta MC. 2023. Chromosome-level organization of the regulatory genome in the Drosophila nervous system. Cell, 25, S0092-8674, 00741-9. http://doi.org/10.1016/j.cell.2023.07.008

Nitabach, M. N. (2006). Electrical Hyperexcitation of Lateral Ventral Pacemaker Neurons Desynchronizes Downstream Circadian Oscillators in the Fly Circadian Circuit and Induces Multiple Behavioral Periods. *Journal of Neuroscience*, *26*, 479–489. https://doi.org/10.1523/jneurosci.3915-05.2006

O'Hare, J. K., Gonzalez, K. C., Herrlinger, S. A., Hirabayashi, Y., Hewitt, V. L., Blockus, H., Szoboszlay, M., Rolotti, S. V, Geiller, T. C., Negrean, A., Chelur, V.,

Polleux, F., & Losonczy, A. (2022). Compartment-specific tuning of dendritic feature selectivity by intracellular Ca2+ release. *Science*, *375*. https://doi.org/10.1126/science.abm1670

Owald, D., Felsenberg, J., Talbot, C. B., Das, G., Perisse, E., Huetteroth, W., & Waddell, S. (2015). Activity of Defined Mushroom Body Output Neurons Underlies Learned Olfactory Behavior in Drosophila. *Neuron*, *86*, 417–427. https://doi.org/10.1016/j.neuron.2015.03.025

Pathak, T., Agrawal, T., Richhariya, S., Sadaf, S., & Hasan, G. (2015). Store-Operated Calcium Entry through Orai Is Required for Transcriptional Maturation of the Flight Circuit in *Drosophila*. *The Journal of Neuroscience*, *35*, 13784–13799. https://doi.org/10.1523/jneurosci.1680-15.2015

Ping, Y., Waro, G., Licursi, A., Smith, S., Vo-Ba, D.-A., & Tsunoda, S. (2011). Shal/Kv4 Channels Are Required for Maintaining Excitability during Repetitive Firing and Normal Locomotion in Drosophila. *PLoS ONE*, *6*, e16043. https://doi.org/10.1371/journal.pone.0016043

Postma, M., & Goedhart, J. (2019). PlotsOfData—A web app for visualizing data together with their summaries. *PLOS Biology*, *17*, e3000202. https://doi.org/10.1371/journal.pbio.3000202

Prakriya, M., & Lewis, R. S. (2015). STORE-OPERATED CALCIUM CHANNELS. *Physiol Rev*, *307*, 1383–1436. https://doi.org/10.1152/physrev.00020.2014

Ramírez, F., Ryan, D. P., Grüning, B., Bhardwaj, V., Kilpert, F., Richter, A. S., Heyne, S., Dündar, F., & Manke, T. (2016). deepTools2: a next generation web server for deep-sequencing data analysis. *Nucleic Acids Research*, *44*(W1), W160–W165. https://doi.org/10.1093/nar/gkw257

Ravi P, Trivedi D, Hasan G. (2018). FMRFa receptor stimulated Ca2+ signals alter the activity of flight modulating central dopaminergic neurons in Drosophila melanogaster. Barsh GS, ed. *PLOS Genet*, 14:e1007459. http://doi.org/10.1371/journal.pgen.1007459

Richhariya, S., Jayakumar, S., Abruzzi, K., Rosbash, M., & Hasan, G. (2017). A pupal transcriptomic screen identifies Ral as a target of store-operated calcium entry in Drosophila neurons. *Scientific Reports*, *7*(1), 1–12. https://doi.org/10.1038/srep42586

1275 Riemensperger, T., Völler, T., Stock, P., Buchner, E., & Fiala, A. (2005). Punishment
1276 Prediction by Dopaminergic Neurons in Drosophila. *Current Biology*, *15*, 1953–
1277 1960. https://doi.org/10.1016/j.cub.2005.09.042
1278 Ritchie, M. E., Phipson, B., Wu, D., Hu, Y., Law, C. W., Shi, W., & Smyth, G. K.
1279 (2015). limma powers differential expression analyses for RNA-sequencing and
1280 microarray studies. *Nucleic Acids Research*, *43*, e47–e47.
1281 https://doi.org/10.1093/nar/gkv007
1282 Robinson, M. D., McCarthy, D. J., & Smyth, G. K. (2009). edgeR: A Bioconductor
1283 package for differential expression analysis of digital gene expression data.
1284 *Bioinformatics*, *26*(1), 139–140. https://doi.org/10.1093/bioinformatics/btp616
1285 Rosenberg, S. S., & Spitzer, N. C. (2011). Calcium Signaling in Neuronal
1286 Development. *Cold Spring Harbor Perspectives in Biology*, *3*, a004259–
1287 a004259. https://doi.org/10.1101/cshperspect.a004259
1288 Sachse S, Rueckert E, Keller A, Okada R, Tanaka NK, Ito K, Vosshall LB. (2007).
1289 Activity-dependent plasticity in an olfactory circuit. Neuron, 56, 838-50.
1290 http://doi.org/10.1016/j.neuron.2007.10.035
1291 Schindelin, J., Arganda-Carreras, I., Frise, E., Kaynig, V., Longair, M., Pietzsch, T.,
1292 Preibisch, S., Rueden, C., Saalfeld, S., Schmid, B., Tinevez, J. Y., White, D. J.,
1293 Hartenstein, V., Eliceiri, K., Tomancak, P., & Cardona, A. (2012). Fiji: An open-
1294 source platform for biological-image analysis. *Nature Methods*, *9*(7), 676–682.
1295 https://doi.org/10.1038/nmeth.2019
1296 Shakiryanova, D., Morimoto, T., Zhou, C., Chouhan, A. K., Sigrist, S. J., Nose, A.,
1297 Macleod, G. T., Deitcher, D. L., & Levitan, E. S. (2011). Differential Control of
1298 Presynaptic CaMKII Activation and Translocation to Active Zones. *Journal of*
1299 *Neuroscience*, *31*, 9093–9100. https://doi.org/10.1523/jneurosci.0550-11.2011
1300 Sharma, A., & Hasan, G. (2020). Modulation of flight and feeding behaviours
1301 requires presynaptic IP3Rs in dopaminergic neurons. *ELife*, *9*.
1302 https://doi.org/10.7554/elife.62297
1303 Shimojima, T. (2003). Drosophila FACT contributes to Hox gene expression through
1304 physical and functional interactions with GAGA factor. *Genes & Development*,
1305 *17*(13), 1605–1616. https://doi.org/10.1101/gad.1086803
1306 Singh, S., & Wu, C. F. (1990). Properties of potassium currents and their role in

membrane excitability in Drosophila larval muscle fibers. *Journal of Experimental Biology*, *152*, 59–76. https://doi.org/10.1242/jeb.152.1.59

Somasundaram, A., Shum, A. K., McBride, H. J., Kessler, J. A., Feske, S., Miller, R. J., & Prakriya, M. (2014). Store-Operated CRAC Channels Regulate Gene Expression and Proliferation in Neural Progenitor Cells. *Journal of Neuroscience*, *34*, 9107–9123. https://doi.org/10.1523/jneurosci.0263-14.2014

Spitzer, N. C. (2012). Activity-dependent neurotransmitter respecification. *Nature Reviews Neuroscience*, *13*, 94–106. https://doi.org/10.1038/nrn3154

Stabell, M., Larsson, J., Aalen, R. B., & Lambertsson, A. (2007). Drosophila dSet2 functions in H3-K36 methylation and is required for development. *Biochemical and Biophysical Research Communications*, *359*, 784–789. https://doi.org/10.1016/j.bbrc.2007.05.189

Streb, H., Bayerdörffer, E., Haase, W., Irvine, R. F., & Schulz, I. (1984). Effect of inositol-1,4,5-trisphosphate on isolated subcellular fractions of rat pancreas. *The Journal of Membrane Biology*, *81*, 241–253. https://doi.org/10.1007/bf01868717

Sugie, A., Marchetti, G., & Tavosanis, G. (2018). Structural aspects of plasticity in the nervous system of Drosophila. *Neural Development*, *13*. https://doi.org/10.1186/s13064-018-0111-z

Sun, F., Zeng, J., Jing, M., Zhou, J., Feng, J., Owen, S. F., Luo, Y., Li, F., Wang, H., Yamaguchi, T., Yong, Z., Gao, Y., Peng, W., Wang, L., Zhang, S., Du, J., Lin, D., Xu, M., Kreitzer, A. C., … Li, Y. (2018). A Genetically Encoded Fluorescent Sensor Enables Rapid and Specific Detection of Dopamine in Flies, Fish, and Mice. *Cell*, *174*, 481-496.e19. https://doi.org/10.1016/j.cell.2018.06.042

Sweeney, S. T., Broadie, K., Keane, J., Niemann, H., & O'Kane, C. J. (1995). Targeted expression of tetanus toxin light chain in Drosophila specifically eliminates synaptic transmission and causes behavioral defects. *Neuron*, *14*, 341–351. https://doi.org/10.1016/0896-6273(95)90290-2

Taber, K. H., & Hurley, R. A. (2014). Volume Transmission in the Brain: Beyond the Synapse. *The Journal of Neuropsychiatry and Clinical Neurosciences*, *26*, iv–4. https://doi.org/10.1176/appi.neuropsych.13110351

Takechi, H., Eilers, J., & Konnerth, A. (1998). A new class of synaptic response involving calcium release in dendritic spines. *Nature*, *396*, 757–760.

https://doi.org/10.1038/25547

Tang, X., Li, T., Liu, S., Wisniewski, J., Zheng, Q., Rong, Y., Lavis, L. D., & Wu, C. (2022). Kinetic principles underlying pioneer function of GAGA transcription factor in live cells. *Nature Structural & Molecular Biology*, *29*, 665–676. https://doi.org/10.1038/s41594-022-00800-z

Thillaiappan, N. B., Chakraborty, P., Hasan, G., & Taylor, C. W. (2019). IP3 receptors and Ca2+ entry. *Biochimica et Biophysica Acta (BBA) - Molecular Cell Research*, *1866*, 1092–1100. https://doi.org/10.1016/j.bbamcr.2018.11.007

Truszkowski, T. L. S., & Aizenman, C. D. (2015). Neurobiology: Setting the Set Point for Neural Homeostasis. *Current Biology*, *25*, R1132–R1133. https://doi.org/10.1016/j.cub.2015.10.021

Tsai, S.-Y., Chang, Y.-L., Swamy, K. B. S., Chiang, R.-L., & Huang, D.-H. (2016). GAGA factor, a positive regulator of global gene expression, modulates transcriptional pausing and organization of upstream nucleosomes. *Epigenetics & Chromatin*, *9*. https://doi.org/10.1186/s13072-016-0082-4

Tsao, C.-H., Chen, C.-C., Lin, C.-H., Yang, H.-Y., & Lin, S. (2018). Drosophila mushroom bodies integrate hunger and satiety signals to control innate food-seeking behavior. *ELife*, *7*. https://doi.org/10.7554/elife.35264

Tsukiyama, T., Becker, P. B., & Wu, C. (1994). ATP-dependent nucleosome disruption at a heat-shock promoter mediated by binding of GAGA transcription factor. *Nature*, *367*(6463), 525–532. https://doi.org/10.1038/367525a0

Venkiteswaran, G., & Hasan, G. (2009). Intracellular Ca2+ signalling and store operated Ca2+ entry are required in Drosophila neurons for flight. *Proceedings of the National Academy of Sciences*, *2009*.

Verma, S. K., Tian, X., LaFrance, L. V, Duquenne, C., Suarez, D. P., Newlander, K. A., Romeril, S. P., Burgess, J. L., Grant, S. W., Brackley, J. A., Graves, A. P., Scherzer, D. A., Shu, A., Thompson, C., Ott, H. M., Aller, G. S. Van, Machutta, C. A., Diaz, E., Jiang, Y., … Miller, W. H. (2012). Identification of Potent, Selective, Cell-Active Inhibitors of the Histone Lysine Methyltransferase EZH2. *ACS Medicinal Chemistry Letters*, *3*, 1091–1096. https://doi.org/10.1021/ml3003346

Viswanath, V., Story, G. M., Peier, A. M., Petrus, M. J., Lee, V. M., Hwang, S. W.,

Patapoutian, A., & Jegla, T. (2003). Opposite thermosensor in fruitfly and mouse. *Nature*, *423*, 822–823. https://doi.org/10.1038/423822a

Waddell, S. (2016). Neural Plasticity: Dopamine Tunes the Mushroom Body Output Network. *Current Biology*, *26*, R109–R112. https://doi.org/10.1016/j.cub.2015.12.023

Wang, Y., Deng, X., & Gill, D. L. (2010). Calcium Signaling by STIM and Orai: Intimate Coupling Details Revealed. *Science Signaling*, *3*, pe42–pe42. https://doi.org/10.1126/scisignal.3148pe42

Weiss, S., Melom, J. E., Ormerod, K. G., Zhang, Y. V, & Littleton, J. T. (2019). Glial Ca2+signaling links endocytosis to K+ buffering around neuronal somas to regulate excitability. *ELife*, *8*. https://doi.org/10.7554/elife.44186

Wilkins, R. C., & Lis, J. T. (1999). DNA distortion and multimerization: novel functions of the glutamine-rich domain of GAGA factor 1 1Edited by M. Yaniv. *Journal of Molecular Biology*, *285*(2), 515–525. https://doi.org/10.1006/jmbi.1998.2356

Xu, W., & Lipscombe, D. (2001). Neuronal CaV1.3α1 L-Type Channels Activate at Relatively Hyperpolarized Membrane Potentials and Are Incompletely Inhibited by Dihydropyridines. *The Journal of Neuroscience*, *21*, 5944–5951. https://doi.org/10.1523/JNEUROSCI.21-16-05944.2001

Yagi, R., Mabuchi, Y., Mizunami, M., & Tanaka, N. K. (2016). Convergence of multimodal sensory pathways to the mushroom body calyx in Drosophila melanogaster. *Scientific Reports*, *6*. https://doi.org/10.1038/srep29481

Yeromin, A. V, Zhang, S. L., Jiang, W., Yu, Y., Safrina, O., & Cahalan, M. D. (2006). Molecular identification of the CRAC channel by altered ion selectivity in a mutant of Orai. *Nature*, *443*, 226–229. https://doi.org/10.1038/nature05108

Zambelli, F., Pesole, G., & Pavesi, G. (2009). Pscan: finding over-represented transcription factor binding site motifs in sequences from co-regulated or co-expressed genes. *Nucleic Acids Research*, *37*, W247–W252. https://doi.org/10.1093/nar/gkp464

Zhai, B., Villén, J., Beausoleil, S. A., Mintseris, J., & Gygi, S. P. (2008). Phosphoproteome Analysis of Drosophila melanogaster Embryos. *Journal of Proteome Research*, *7*, 1675–1682. https://doi.org/10.1021/pr700696a

Zolin, A., Cohn, R., Pang, R., Siliciano, A. F., Fairhall, A. L., & Ruta, V. (2021). Context-dependent representations of movement in Drosophila dopaminergic reinforcement pathways. *Nature Neuroscience*, *24*, 1555–1566. https://doi.org/10.1038/s41593-021-00929-y

Figures

Figure 1

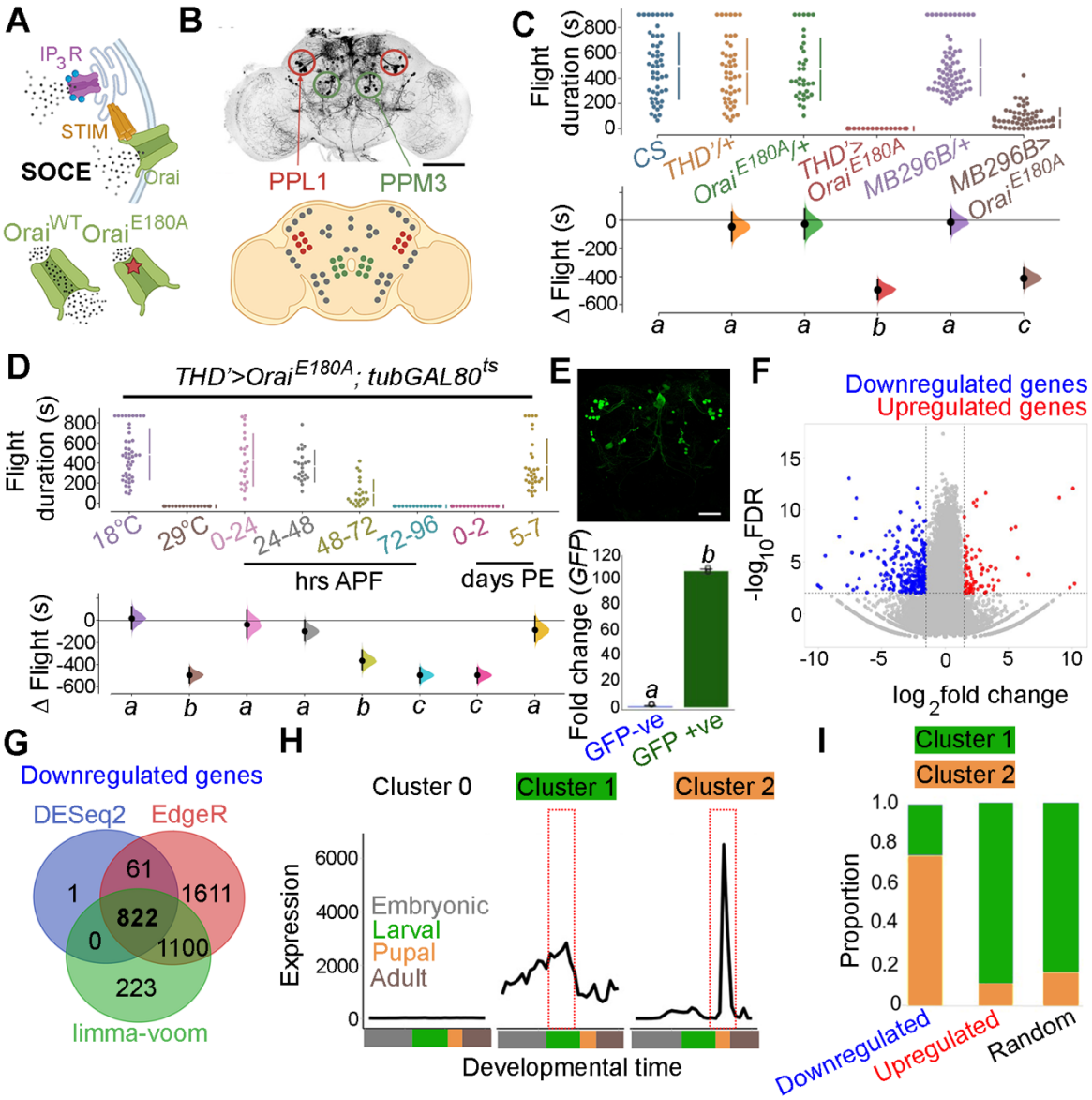

Figure 1. Orai-mediated Ca^{2+} entry sets the gene expression profile of flight-promoting dopaminergic neurons in late development and early adulthood. **A**. A schematic of Ca^{2+} release through the IP_3R and SOCE through STIM/Orai (upper panel) followed by representation of the wildtype (Ca^{2+} permeable) and mutant (Ca^{2+} impermeable) Orai channels (lower panel). **B**. Anatomical location of *THD'* DANs in the fly central brain immunolabelled for mCD8GFP (upper panel) followed by a cartoon of central brain DAN clusters. Scale bar indicates 20 μm. PPL1 and PPM3 clusters are labelled in red and green respectively. **C**. Measurement of flight bout durations

demonstrate a requirement for Orai-mediated Ca^{2+} entry in *THD'* DANs and in 2 pairs of PPL1 DANs marked by the MB296B driver. **D**. *THD*' DANs require Ca^{2+} entry through Orai at 72-96 hours APF and 0-2 days post eclosion to promote flight. In **C** and **D** flight bout durations in seconds (s) are represented as a swarm plot where each genotype is represented by a different color, and each fly as a single data point. The Δ Flight parameter shown below indicates the mean difference for comparisons against the shared Canton S control and is shown as a Cumming estimation plot. Mean differences are plotted as bootstrap sampling distributions. Each 95% confidence interval is indicated by the ends of the vertical error bars. The same letter beneath each distribution refers to statistically indistinguishable groups after performing a Kruskal-Wallis test followed by a post hoc Mann-Whitney U-test ($p<0.005$). At least 30 flies were tested for each genotype. **E**. *THD'* DANs were labelled with cytosolic eGFP (10 μm scale), isolated using FACS and validated for enrichment of *GFP* mRNA by qRT-pCR (lower panel). The qRT-pCR results are from 4 biological replicates with different letters representing statistically distinguishable groups after performing a two-tailed t test ($p<0.05$). **F.** RNA-seq comparison of FAC sorted populations of GFP labelled THD' DANs from *THD'>GFP* and *THD'>GFP;Orai*^{E180A} pupal dissected CNSs. The RNA-Seq data is represented in the form of a volcano plot of fold change vs FDR. Individual dots represent genes, coloured in red (upregulated) or blue (downregulated) by >1 fold. **G.** Downregulated genes were identified by 3 different methods of DEG analysis, quantified and compared as a Venn diagram. **H.** Gene expression trajectories of SOCE-induced DEGs plotted as a function of developmental time (modENCODE Consortium et al., 2010) and clustered into 3 groups using k-means analysis. **I**. The relative proportion of downregulated, upregulated genes, and a random set of genes found in the clusters described in (**H**) indicate that 75% of downregulated genes exhibit a pupal peak of expression.

1452 **Figure 2**

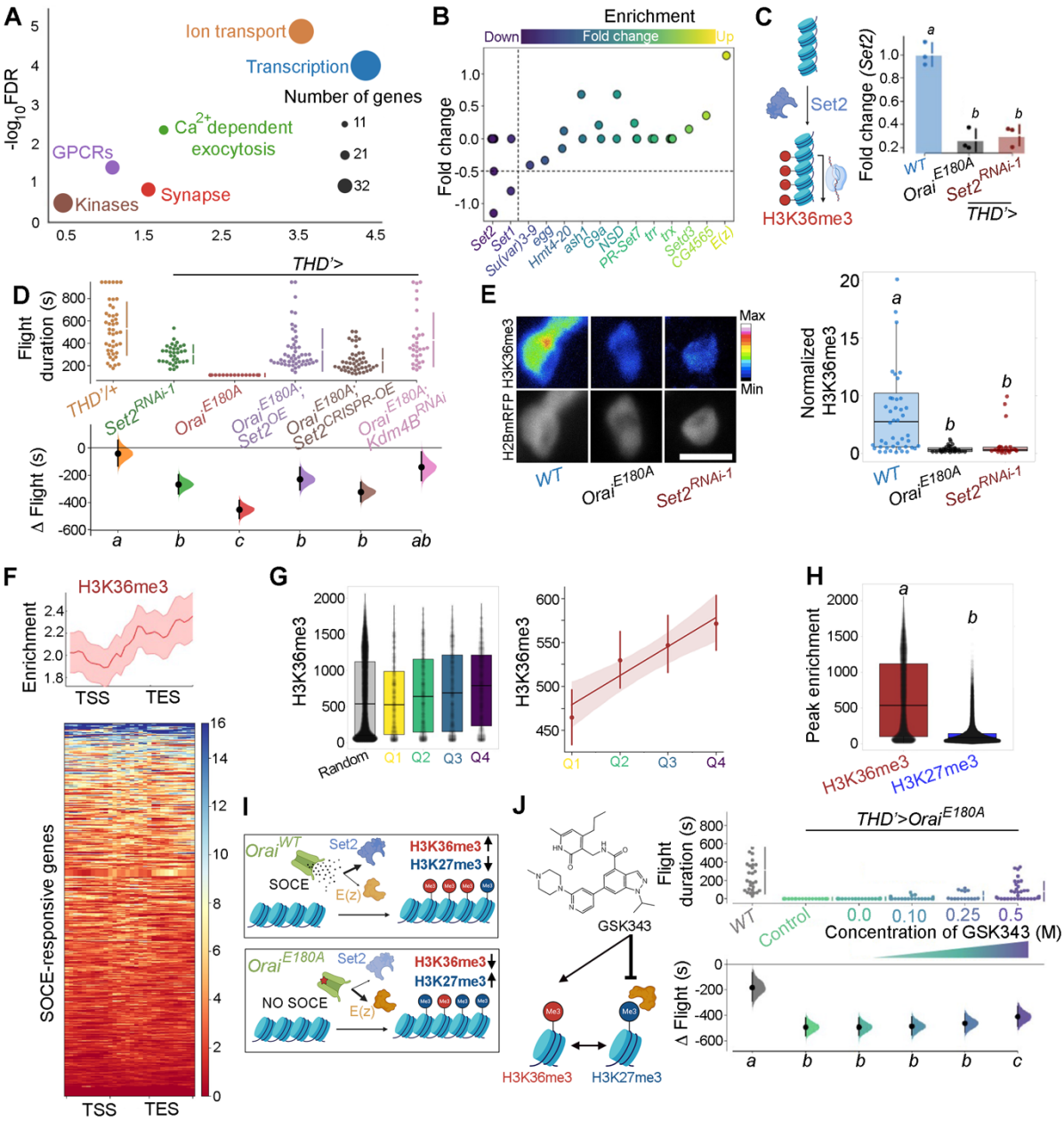

1453 **Figure 2. Ca^{2+} entry through Orai regulates gene expression by Set2-mediated**
1454 **histone modification. A.** Scatterplot of GO categories enriched in SOCE-responsive
1455 genes. Individual GO terms are represented as differently colored circles, with radius
1456 size indicating number of genes enriched in that category. **B.** Fold change of SET
1457 domain containing genes as indicated. Individual circles on the Y-axis for each gene
1458 represent transcript variants pertaining to that gene. **C.** Transcripts of the H3K36
1459 methyltransferase (left) are significantly diminished (right) in *THD'* DANs either upon
1460 loss of Orai function (*THD'>Orai*^{E180A}) or by knockdown of *Set2* (*THD'>Set2*^{RNAi}). qRT-
1461 PCRs were performed from FAC sorted *THD'* DANs with 3 biological replicates.
1462 Individual $2^{-\Delta\Delta CT}$ values are shown as points. Letters represent statistically
1463 distinguishable groups after performing an ANOVA and post hoc Tukey test ($p<0.05$).
1464 **D.** Significant rescue of flight bout durations seen in *THD' > Orai*^{E180A} flies by
1465 overexpression of *Set2* and by knockdown of the *Kdm4B* demethylase indicating a net

requirement for H3K36me3. Flight durations of single flies are depicted as swarm plots and the Δ flight parameter is shown below. Both were measured as described in the legend to Figure 1. N = 30 or more flies for each genotype. Letters represent statistically distinguishable groups after performing an ANOVA and post hoc Tukey test ($p<0.005$) **E**. Representative images (upper panel) and quantification (lower panel) from immunostaining of H3K36me3 and H2BmRFP in nuclei of *THD'* DANs from at least 10 brains. Scale bar represents 5 μm. The boxplot represents individual H3K36me3/H2BmRFP ratios from each *THD'* DAN for each genotype. Letters represent statistically distinguishable groups after performing an ANOVA and post hoc Tukey test ($p<0.05$) **F**. H3K36me3 enrichment over the gene bodies of SOCE-responsive genes in wildtype fly heads represented in the form of a tag density plot. **G**. H3K36me3 signal is enriched on WT SOCE-responsive genes with greater downregulation upon loss of Orai function. Individual data points represent *WT* H3K36me3 ChIP-Seq signals from adult fly heads represented as a boxplot (left) and a regression plot (right; Pearson's correlation coefficient = 0.11) indicating a correlation between extent of downregulation upon loss of SOCE and greater enrichment of H3K36me3. **H**. SOCE-responsive genes are enriched in H3K36me3 signal as compared to H3K27me3 signal as measured from relevant ChIP-Seq datasets. Adult fly head ChIP-Seq datasets for measurements in **F** to **H** were obtained from modEncode (modENCODE Consortium et al., 2010). **I**. Schematic representation of how Orai mediated Ca^{2+} entry regulates a balance of two opposing epigenetic signatures in developing DANs. **J**. Pharmacological inhibition of H3K27me3 using GSKS343 (left) in *THD'>Orai*^{E180A} flies results in a dose-dependent rescue of flight bout durations (right). Flight assay measurements from N> 30 flies, are represented as described earlier. Letters represent statistically distinguishable groups after performing an ANOVA and post hoc Tukey test ($p<0.005$).

1501 **Figure 3**

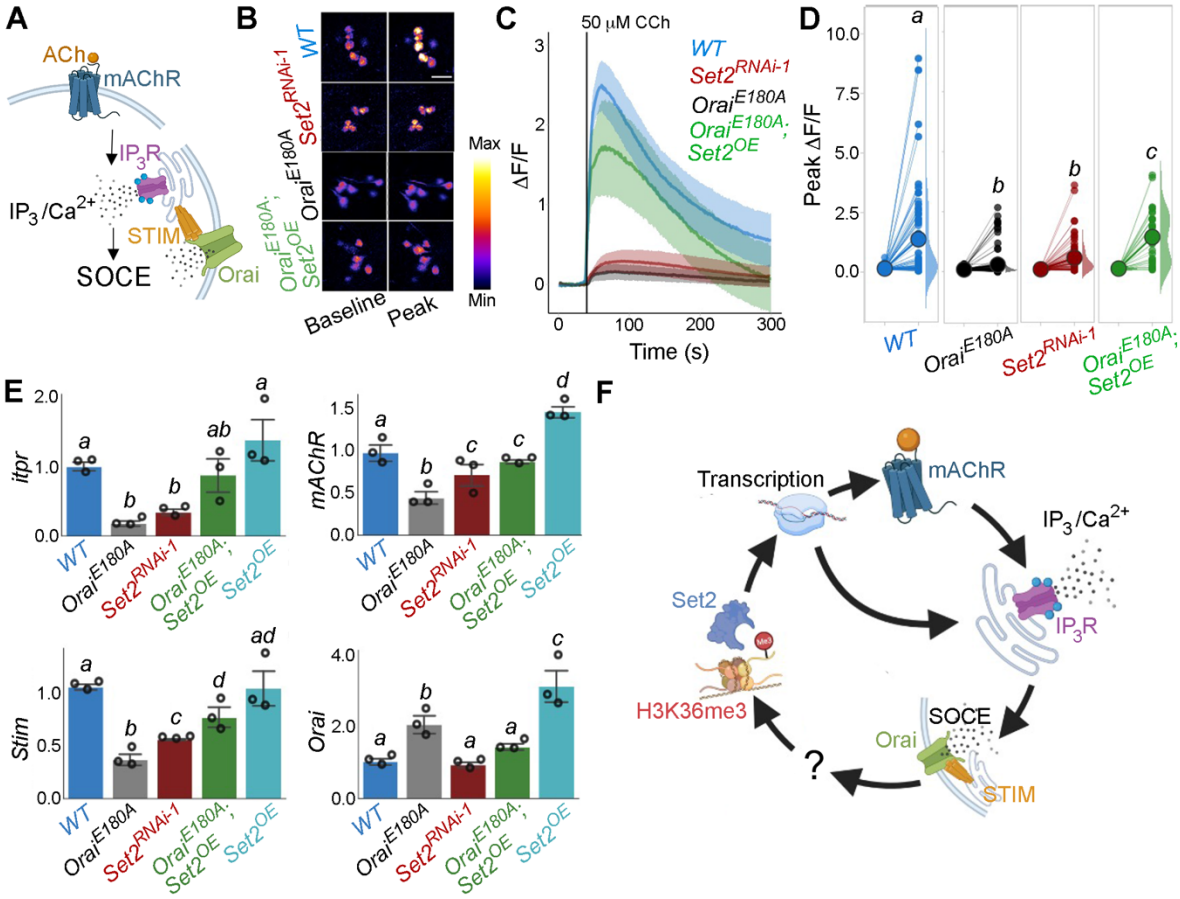

1502 **Figure 3. Orai-mediated Ca^{2+} entry potentiates cellular Ca^{2+} responses to**
1503 **cholinergic inputs through Set2 and a transcriptional feedback loop**
1504 **A**. A schematic of intracellular Ca^{2+} signaling downstream of neuromodulatory
1505 signaling where activation of mAChR stimulates intracellular Ca^{2+} release through the
1506 IP_3R followed by SOCE through STIM/Orai. **B.** Cholinergic inputs by addition of
1507 carbachol (CCh) evoke Ca^{2+} signals as measured by change in the fluorescence of
1508 GCaMP6m in *THD'* DANs of ex-vivo brains. Representative GCaMP6m images of
1509 *THD'* DANs are shown with baseline and peak evoked responses in the indicated
1510 genotypes. Scale bar = 10 μM. **C**. Median GCaMP6m responses plotted as a function
1511 of time. A shaded region around the solid line represents the 95% confidence interval
1512 from 4-5 cells imaged per brain from 10 or more brains per genotype. **D.** Individual
1513 cellular responses depicted as a paired plot where different letters above indicate
1514 statistically distinguishable groups after performing a Kruskal Wallis Test and a Mann-
1515 Whitney U-test ($p<0.05$). **E**. qRT-PCR measurements of *itpr*, *mAChR*, *Stim* and *Orai*
1516 from FAC sorted *THD'* DANs obtained from three biological replicates of appropriate
1517 genetic backgrounds. The genotypes include DANs with loss of cellular Ca^{2+}
1518 responses (*THD'>Orai*^{E180A}; and *THD'>Set2*$^{RNAi-1}$), rescue of cellular Ca^{2+} response by
1519 overexpression of *Set2* (*THD'>Orai*^{E180A}; *Set2*^{OE}) and *Set2* overexpression. Bar plots
1520 indicate mean expression levels in comparison to *rp49*, with individual data points
1521 represented as hollow circles. The letters above indicate statistically indistinguishable
1522 groups after performing a Kruskal Wallis Test and a Mann-Whitney U-test ($p<0.05$). **F**.

Schematic representation of a transcriptional feedback loop downstream of cholinergic stimulation in *THD'* DANs.

Figure 4

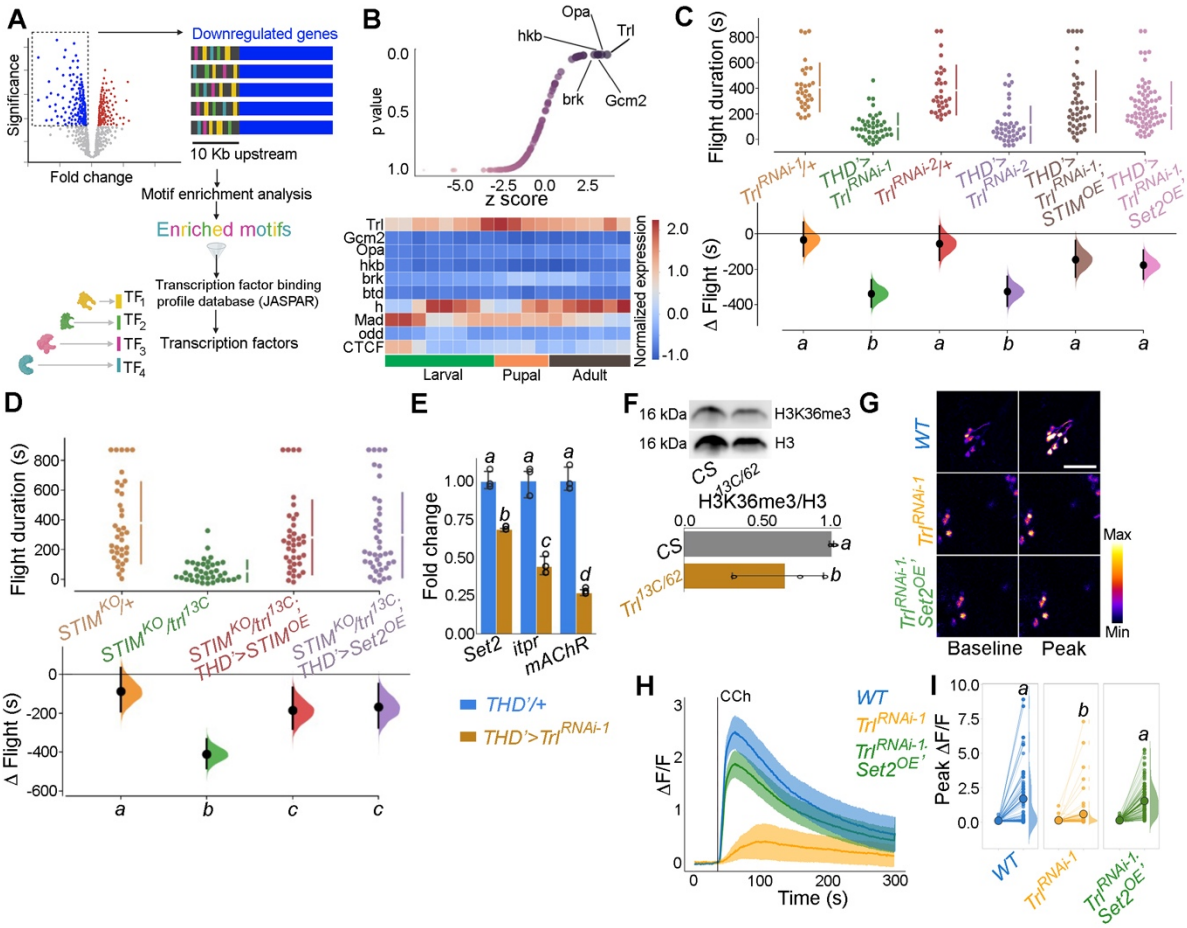

Figure 4. Identification of Trl as an SOCE responsive transcription factor

A. Schematic of motif enrichment analysis for identification of putative SOCE dependent transcription factors (TFs). **B.** Candidate TFs identified (upper panel) and their expression through development (lower panel; modEncode(modENCODE Consortium et al., 2010)) suggests Trl as a top SOCE-responsive candidate TF. **C.** Genetic depletion of *Trl* in *THD'* DANs results in significant flight defects, that can be rescued by overexpression of either *STIM* or *Set2*. **D.** Heteroallelic combination of the *Trl* hypomorphic allele (*trl*^{13C}) with a *STIM* deficiency causes significant flight deficits, that can be rescued by overexpression of *STIM* or *Set2*. **E.** qRT-PCRs measured relative to *rp49* show reduced *Set2, itpr, and mAChR* levels in *THD'* DANs upon *Trl* knockdown with *Trl*$^{RNAi-1}$. Individual data points of 4 biological replicates are shown as circles and mean expression level as a bar plot (± SEM). The letters above indicate statistically indistinguishable groups after performing a Kruskal Wallis Test and a Mann-Whitney U-test ($p<0.05$). **F.** A representative western blot (left) showing reduced H3K36me3 levels in a *Trl* mutant combination. Quantification of H3K36me3 from 3 biological replicates of *WT* (control) and *Trl* mutant brain lysates (panel on the right). Letters indicate statistically indistinguishable groups after performing a two-tailed t-test ($p<0.05$). **G.** Knockdown of *Trl* in *THD'* neurons attenuate Ca^{2+} response to CCh as shown in representative images of GCamP6m fluorescence quantified in (**H-I**).

Scale bar = 10 μM. *Set2* overexpression in the background of *THD'>Trl*^{RNAi} rescues the cholinergic response (**G-I**). Quantification of Ca^{2+} responses are from 10 or more brains per genotype and were performed as described in the legend to Figure 3. The letters above indicate statistically indistinguishable groups after performing a Kruskal Wallis Test and a Mann-Whitney U-test (p<0.05).

Figure 5

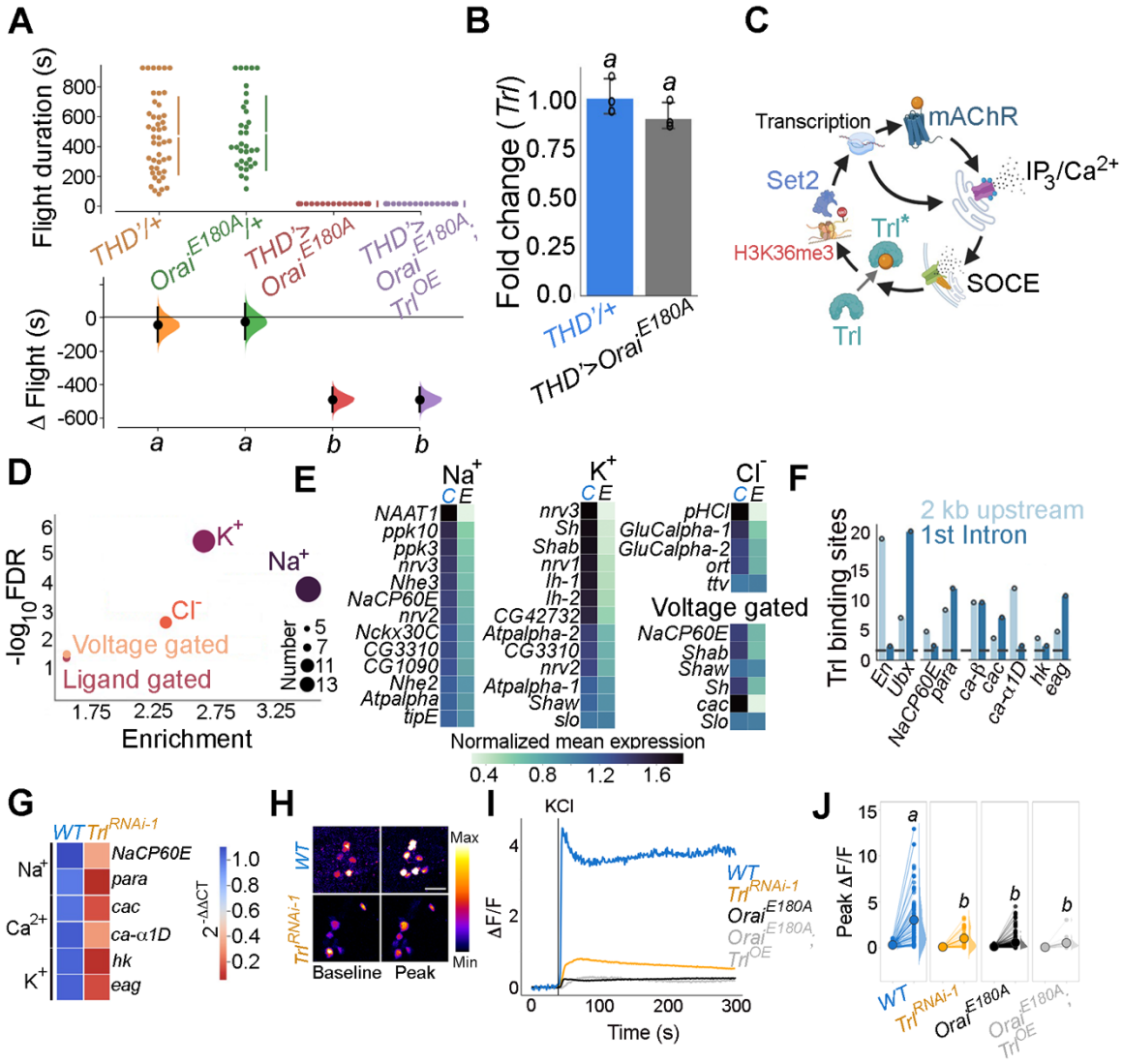

Figure 5. **Trl activity downstream of SOCE is required for *THD'* DAN activity**. A. Overexpression of *WT Trl* is insufficient to rescue flight deficits in *THD'>Orai*^{E180A} flies as evident from flight bout measurements in the indicated genotypes. Flight assay measurements are as described earlier. **B**. *Trl* transcript levels are not altered in *THD'>Orai*^{E180A} neurons with loss of SOCE. qRT-PCR data are measured relative to *rp49*. The bar plot indicates mean expression levels, with individual data points represented as circles. The letters above indicate statistically indistinguishable groups from 3 independent biological replicates after performing a two-tailed t-test (p<0.05). **C**. Schematic with possible Ca^{2+} - mediated activation of Trl downstream of Orai-mediated Ca^{2+} entry (SOCE). **D.** Genes encoding ion channels are enriched among SOCE responsive genes in *THD'* DANs as determined by GO analysis. Circles of

varying radii are scaled according to the number of genes enriched in that category. **E**. Downregulation of individual ion channel genes depicted as a heatmap. **F**. Number of Trl binding sites (GAGA repeats) shown as a bar plot in the regulatory regions (2 kb upstream or 1st intron) of key SOCE-responsive ion channel genes compared to known Trl targets (*En* and *Ubx*). The dashed line indicates the average expected number of Trl targets. **G**. Heatmap of 2^-ΔΔCT values measured using qRT-PCRs from sorted *THD'* DANs with knockdown of *Trl*. **H.** Representative images of KCl-induced depolarizing responses in *THD'* DANs with knockdown of *Trl*. (Scale bar = 10 μM) quantified in **I and J**. Quantification of Ca^{2+} responses are from 10 or more brains per genotype and were performed as described in the legend to Figure 3. The letters above indicate statistically indistinguishable groups after performing a Kruskal Wallis Test and a Mann-Whitney U-test (p<0.05).

Figure 6

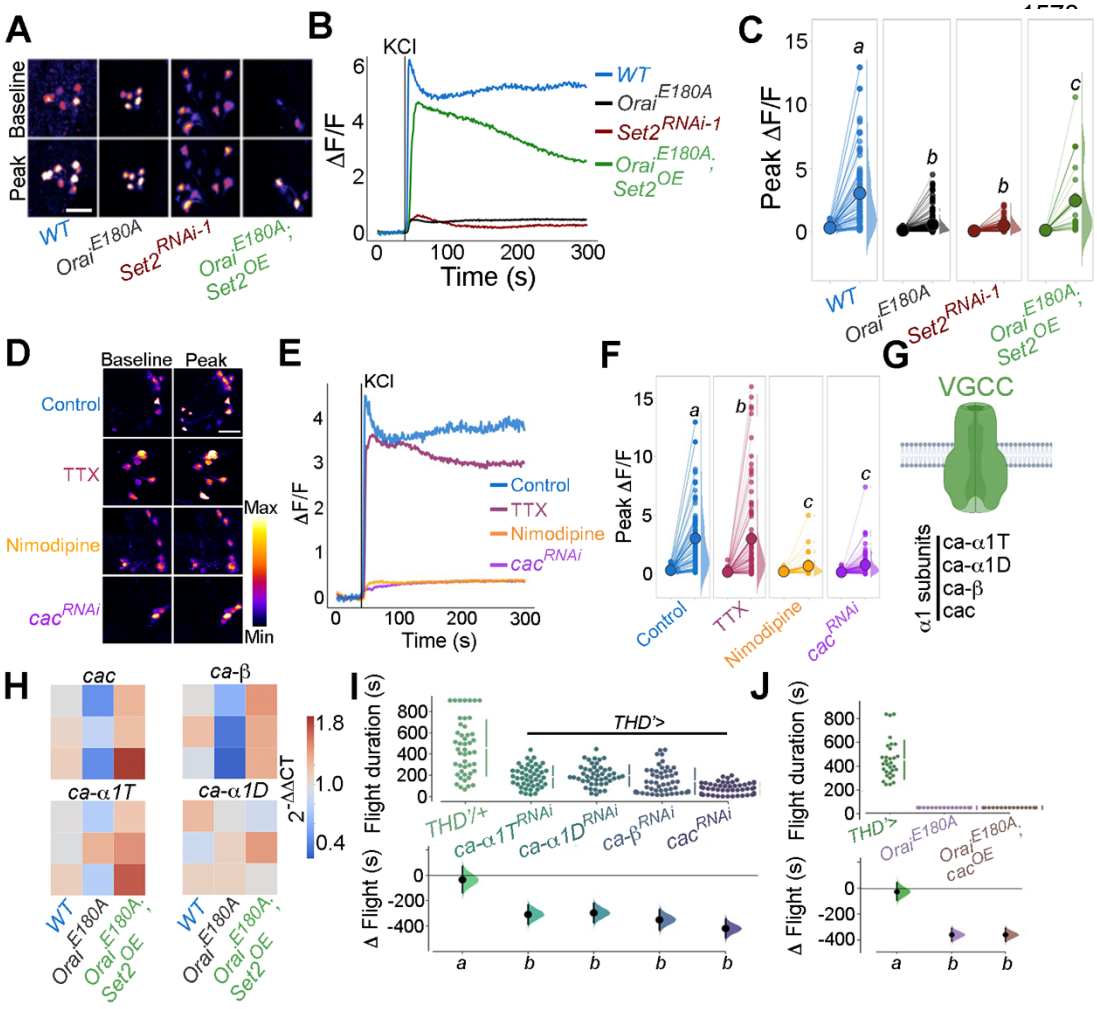

Figure 6. fpDAN excitability requires Orai-mediated Ca^{2+} entry acting through *Set2* -mediated VGCC gene expression. KCl-induced depolarizing responses in *fp*DANs of the indicated genotypes measured using GCaMP6m indicate a requirement for Orai and *Set2*. Representative images **A. (**scale bar = 10 μM), quantified in **B.** and **C**. KCl evoked responses are modulated upon treatment with 10 μM TTX (magenta), 10 μM Nimodipine (orange), and upon *cac*^{RNAi} (purple)- representative images (scale bar = 10 μM), (**D**), quantified in **E**. Median KCl-evoked GCaMP6m responses plotted

as a function of time. The solid line indicates the time point of addition of 70 mM KCl. KCl responses are quantified as a paired plot of peak responses and **F**. with letters representing statistically indistinguishable groups as measured using a Kruskall Wallis test and post hoc Mann-Whitney U test ($p<0.05$). Quantification of Ca^{2+} responses are from 10 or more brains per genotype and were performed as described in the legend to Figure 3. **G.** Schematic of a typical VGCC and its constituent subunits. **H.** Heatmap of 2^-ΔΔCT values measured using qRT-PCRs from sorted *THD'* DANs show a reduction in the expression of VGCC subunit genes upon loss of Orai function and a rescue by *Set2* overexpression. **I**. Flight assays representing the effect of various VGCC subunit gene RNAis showing flight defects to varying extents. Overexpression of the key VGCC subunit gene-*cac* is required (**I**) but not sufficient (**J**) for restoring flight defects caused by loss of *Orai* function. Flight assay measurements are as described earlier.

Figure 7

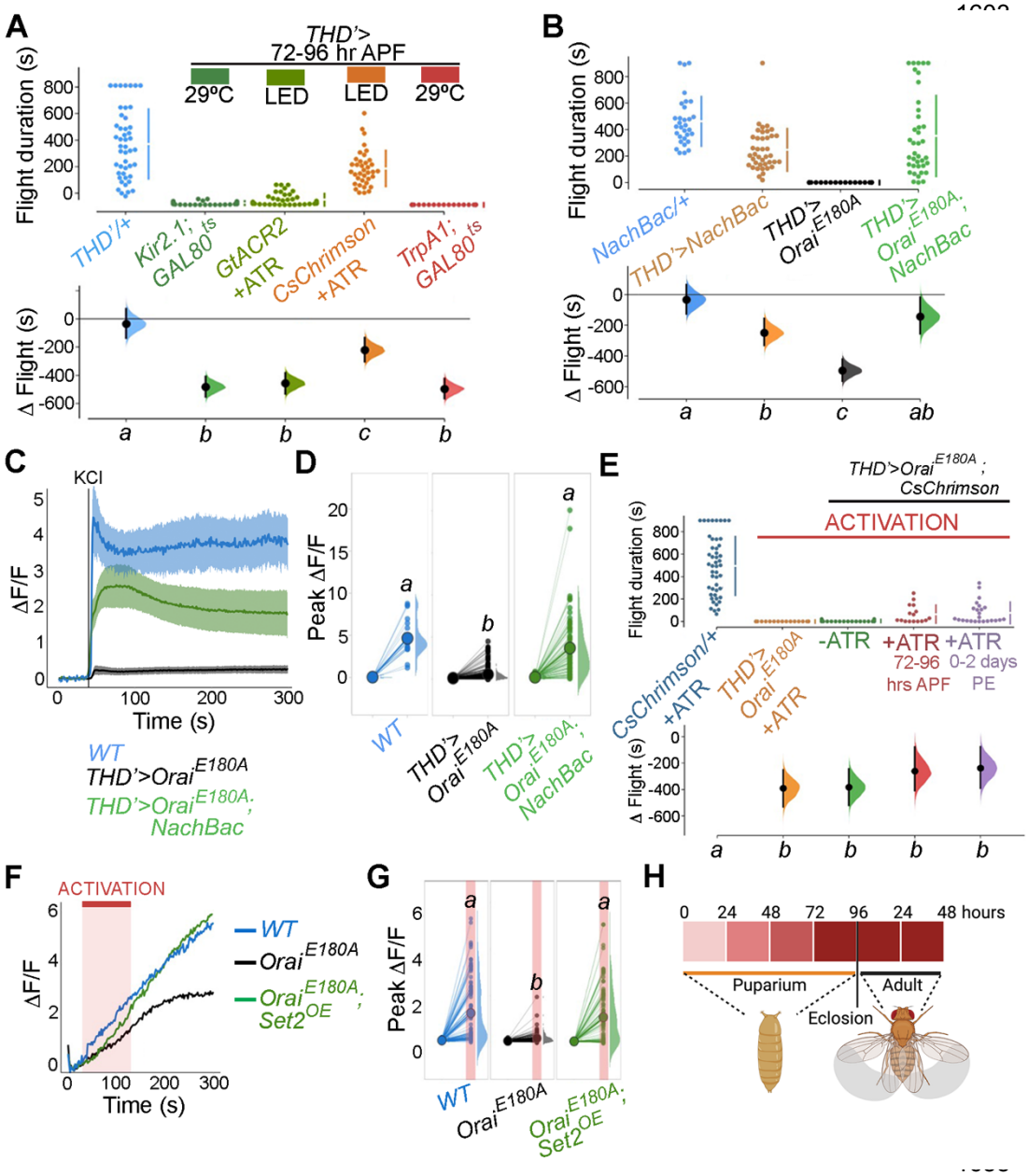

Figure 7. SOCE-mediated gene expression sets the excitability threshold during pupal development **A.** Altering excitability in *THD'* DANs using *Kir2.1* or *GtACR2* mediated inhibition or *CsChrimson* or *TrpA1* during the critical 72-96 hour APF developmental window results in significant flight defects. Orai loss of function phenotypes can be rescued by overexpression of *NachBac* or *CsChrimson* in terms of flight bout durations (**B, E**) and depolarizing KCl responses (**C, D, D, G**). **H.** Schematic for Orai-mediated Ca^{2+} entry regulating expression of key genes that regulate the excitability threshold of dopaminergic neurons regulating flight during a critical developmental window. Flight assays are represented as described earlier, (n>30). Ca^{2+} responses were quantified as described in the legend to Figure 3 and were from 10 or more brains per genotype. Letters above each genotype represent statistically indistinguishable groups as measured using a Kruskall-Wallis test and post hoc Tukey test (p<0.05).

Figure 8

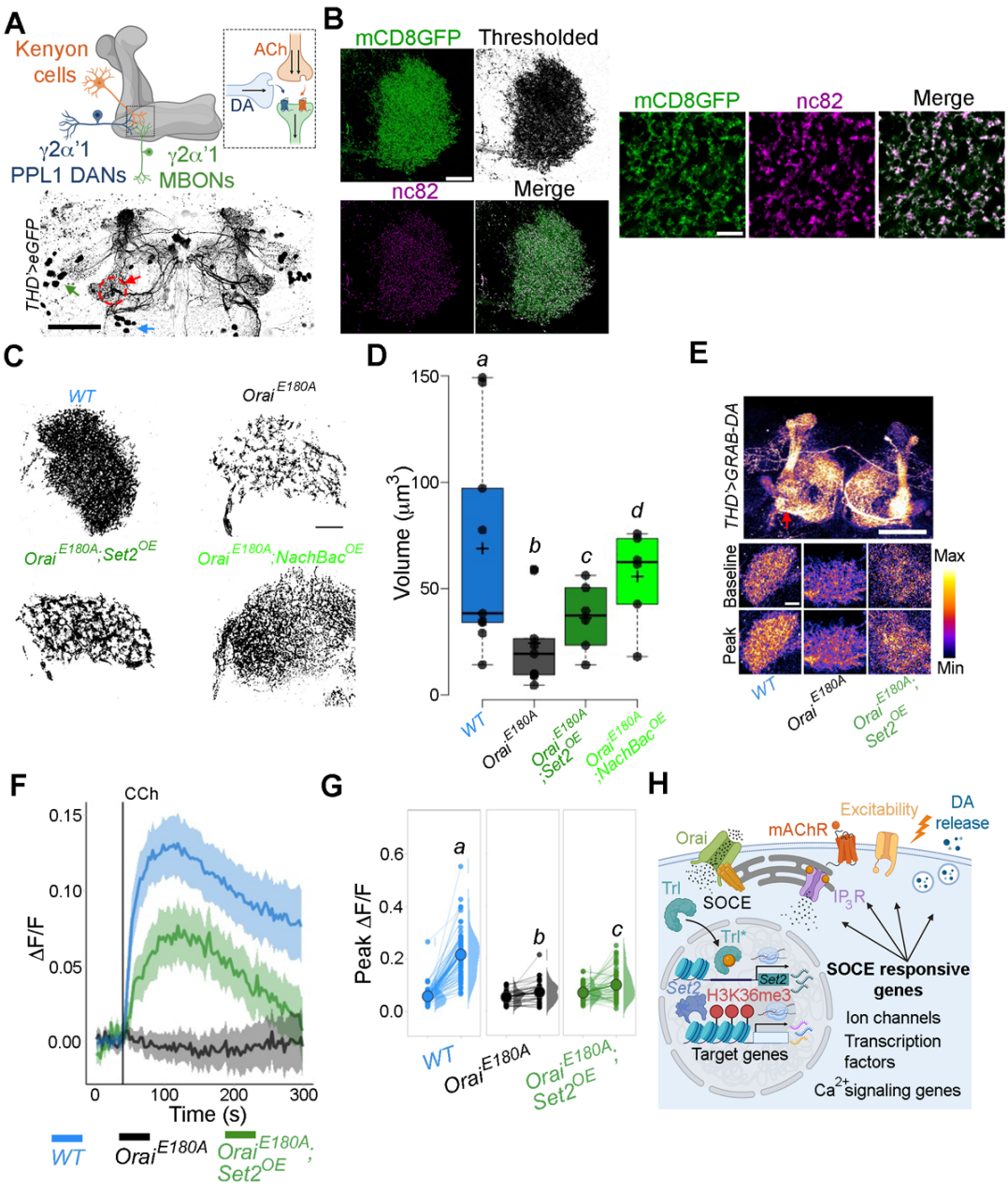

1683 **Figure 8. *THD'* DANs require SOCE-mediated gene expression for axonal**
1684 **arborization and neuromodulatory dopamine release in the mushroom body γ**
1685 **lobe. A.** Schematic of a KC-DAN-MBON tripartite synapse at the γ2α'1 MB lobe
1686 (upper), innervated by fpDANs (lower). The γ2α'1 MB lobe is marked by a red circle
1687 and arrow and the fpDAN clusters are marked with a green arrow (PPL1) and blue
1688 arrow (PPM3) . Scale bar=50 μM. **B**. Representative images of the mushroom body γ
1689 lobe marked with THD' driven mCD8GFP (green) and immunolabelled with anti-nc82
1690 (Brp) antibody (magenta) to mark the presynaptic terminals. Scale bar = 5 μm. **C**.
1691 Representative optical sections through the mushroom body γ lobe from the indicated
1692 genotypes. Changes in axonal arborization observed were quantified as total
1693 projection volume in **D**. **E**. CCh-evoked DA release measured at the γ2α'1 MB lobe
1694 using the GRAB-DA sensor expressed in *THD'* DANs. Representative GRAB-DA
1695 images of *THD'* DANs are shown with baseline and peak evoked responses in the
1696 indicated genotypes. Scale bar = 10 μM. **F**. Median GRAB-DA responses plotted as a
1697 function of time. A shaded region around the solid line represents the 95% confidence
1698 interval from 10 or more brains per genotype. **G.** Individual cellular responses depicted
1699 as a paired plot of peak responses where different letters above indicate statistically
1700 distinguishable groups after performing a Kruskal Wallis Test and a Mann-Whitney U-
1701 test. **H**. Schematic describing how Orai-mediated Ca^{2+} entry regulates expression of
1702 key genes that control neuronal activity in fpDANs.